62-3-5

MAGNETOGASDYNAMIC THRUST VECTORING OF ROCKET MOTORS

DANIEL E. ROSNER

February 1962

AeroChem Research Laboratories, Inc.
a subsidiary of PFAUDLER PERMUTIT INC.
Princeton, New Jersey

Prepared for
BUREAU OF NAVAL WEAPONS
Department of the Navy
Contract NOw-60-0536-c

MAGNETOGASDYNAMIC THRUST VECTORING OF ROCKET MOTORS, INCLUDING THE EFFECTS OF FINITE ELECTRON-ION RECOMBINATION KINETICS

A Parametric Study

Daniel E. Rosner

AeroChem Research Laboratories, Inc.
Princeton, New Jersey

a subsidiary of Pfaudler-Permutit Inc.

Prepared for

BUREAU OF NAVAL WEAPONS
Department of the Navy
Contract NOw-60-0536-c

SUMMARY

Universal curves are presented to facilitate the prediction of magnetohydrodynamic control forces in rocket motor practice. A set of equilibrium calculations also required for this purpose is presented for 21 rocket propellant combinations with alkali atom seeding. Since the nozzle expansion process can lead to electrical conductivities at the exit section much larger than those corresponding to local ionization equilibrium, a graphical method is introduced and discussed which enables quantitative estimates to be made of the extent of this nonequilibrium enhancement as well as the conditions under which it can be ignored. By combining this material it is possible to extract general information as to the independent factors favoring maximum exhaust jet interaction with the applied magnetic field. Some of the major factors (other than large field strength) giving rise to favorable conditions are a) presence of low ionization potential materials in "hot" chambers, b) small values of the effective specific heat ratio, c) moderate rather than extremely large chamber pressures, and d) large physical size. It appears, from the calculations carried out thus far, that control forces of the order of 0.1 to 1.0 percent of the gross thrust are attainable by applying large magnetic fields (10,000 to 30,000 gauss) to the exhaust jets of rocket motors in the 10,000 lb thrust class, which have been seeded with alkali atoms to the extent of 0.1 to 1.0 percent by mass. With the use of superconducting magnet coils, larger field strengths are possible (perhaps up to 100,000 gauss) and side thrusts of the order of several percent of the gross thrust are predicted. Because of competing factors, these control force expectations generally apply to both the equilibrium as well as nonequilibrium cases envisioned.

ACKNOWLEDGEMENTS

The author wishes to thank Dr. C. Boyars for suggesting the problem and Dr. H. F. Calcote for providing the opportunity to discuss many of its controversial aspects. He is also particularly indebted to F. Kuehner for carrying out the bulk of the numerical calculations presented herein, and to the many authors whose work is implicitly or explicitly represented in the bibliography for providing the groundwork which made this study possible.

TABLE OF CONTENTS

TABLE OF CONTENTS (CON'T)

LIST OF TABLES

LIST OF FIGURES

LIST OF FIGURES (CON'T)

NOMENCLATURE

A	cross-sectional area at a station in the nozzle
$\bar{A}$	$A/A_t = (d/d_t)^2$
B	magnetic field strength
c	ideal exhaust velocity
c*	characteristic velocity of propellant
C_r	ion recombination rate parameter; Eq. (18)
Cs	chemical symbol for the element cesium
d	diameter of cross-section
D_t	throat diameter ($= d_t$)
e	electronic charge
ΔE^o	energy change across ionization reaction
E	equilibrium expansion factor; Eq. (11)
F	thrust
G	universal function defined by Eq. (C-9)
h	Planck's constant
H	function of Mach number defined by Eq. (B-28)
I_{sp}	specific impulse (thrust per unit weight flow) of a rocket motor
k	Boltzmann's constant

NOMENCLATURE (CON'T)

K_p	equilibrium constant; Eq. (6)
K	chemical symbol for potassium
L	effective length of the magnetic field in the axial direction
M	Mach number
m	mass of the electron
$\dot{m}$	mass flow rate
$\mathfrak{M}$	molecular weight
n	number density
$\bar{n}$	n/n_c
p	total pressure
$\bar{p}$	p/p_c
Q	magnetogasdynamic interaction parameter; Eq. (1)
Q_σ	effective collision cross-section
R	universal gas constant
S	represents seed species
T	absolute temperature
$\bar{T}$	T/T_c
u	streamwise velocity
$\bar{u}$	u/c^*
$\dot{w}$	mass rate of production per unit volume (source term); Eq. (15)
X	nondimensional axial position [Eq. (5)]
X_i	mole fraction of species i in mixture [Eq. (2)]
$\bar{X}_i$	$X_i/X_{i,c}$
x	distance in axial direction
Y	mass fraction [Eq. (B-6)] or nondimensional transverse position [Eq. (A-5)]
y	distance in transverse direction

Greek

α	mass fraction of seed material added
α_r	ion recombination coefficient; Eq. (15)
γ	specific heat ratio of carrier gas ($\gamma \equiv c_p/c_v$)
θ	inclination angle between imposed magnetic field and nozzle axis
Θ	characteristic temperature for ionization; Table I
ρ	total density
σ	electrical conductivity; Eq. (2)

NOMENCLATURE (CON'T)

Σ	nonequilibrium enhancement, σ/σ_{eq}; Eq. (C-3)
τ	characteristic time or nondimensional time; Eq. (A-5)
Φ	divergance half angle of conical expansion section
ω_T	exponent on temperature in the recombination coefficient law; Eq. (16)
ω_p	exponent on pressure in the recombination coefficient law; Eq. (16)
ν	angle parameter in Eqs. (B-15), (B-16)

Subscripts

+	pertaining to positive ions
$\perp$	in transverse direction
o	undisturbed (without magnetic field); at time = 0; or at some arbitrary initial point in nozzle [see Eq. (B-27)]
*	pertaining to sonic conditions (Mach number = unity)
c	in the combustion chamber
Cs	pertaining to the element cesium
chem	pertaining to a chemical rate process at the nozzle exit section
e	pertaining to electrons
ex	at the nozzle exit section
eq	pertaining to local thermochemical equilibrium
f	at the freeze point
flow	pertaining to changes due to bodily transport
K	pertaining to the element potassium
m	at the "match" point
p	pertaining to pressure dependence or at constant pressure
r	pertaining to gas phase ion-electron recombination
ref	reference value of quantity in question
s	pertaining to the seed material
t	at the nozzle throat section
T	pertaining to temperature dependence
x	component in x direction
y	component in y direction

Superscripts

+	singly ionized
*	characteristic value of
o	at the standard state

NOMENCLATURE (CON'T)

Miscellaneous

$\propto$	proportional to
$\exp(x)$	the function e^x
Δ	change in or difference of
$\overline{(\ )}$	normalized or dimensionless
$\langle\ \rangle$	spatial average of
$\dot{x}$, $\ddot{x}$	first and second derivatives of x with respect to time
O/F	oxidizer to fuel ratio, by weight
E( )	functional notation
0.0_m1	denotes the number 0.000001, etc.; thus $0.0_mN \equiv N \times 10^{-(m+1)}$

I. INTRODUCTION AND OBJECTIVES

An electrically conducting gas can be subjected to a force when it moves through a stationary magnetic field since electrical currents are induced which can interact with the imposed field. This being the case, it is possible, at least in principle, to use magnetic fields to control the motion of high speed jets, as, for example, would be required in thrust vectoring a propulsion device. Assuming such a technique would have advantages over more conventional control methods,† it becomes necessary to inquire into the nature of the interaction and particularly the magnitude of the magnetic field strengths required to achieve the desired control forces.‡ The results of an investigation of this type are included in the present work, where emphasis will be given to their presentation in a form having sufficient generality to be adaptable to different design needs. Thus, insofar as possible, the problem will be divided into independent aspects governing the magnitude of the anticipated MHD effect for the case of conventional rocket motors expanding the products of combustion reactions. Calculations for a number of representative propellant combinations will be included.

II. EFFECT OF AN INCLINED MAGNETIC FIELD ON TRANSVERSE THRUST

We first imagine a uniform jet of electrically conducting gas passing through an imposed field of strength B inclined at an angle θ to the direction of flow (see Fig. 1). If the jet has a diameter d and the magnetic field has an axial extent L, then a fluid particle trajectory analysis (see Appendix A) can be carried out to determine the anticipated transverse thrust $F_\perp$ obtained for prescribed values of the field length to jet diameter ratio, L/d, and the dimensionless magnetogasdynamic interaction parameter

$$Q \equiv \frac{\sigma B^2 d}{\rho c} \tag{1}$$

---

†Important considerations are mechanical complexity, weight, response, severity of high temperature (materials) problem.

‡Recent developments in solid state physics suggest that superconducting magnet coils[2] may become available which would enable large increases in field strengths over those currently attainable.

Here σ is the electrical conductivity of the partially ionized gas. The product of the gas density ρ with the exhaust velocity c appearing in the denominator will be recognized as momentum of the gas per unit volume. If F_o designates the streamwise thrust in the absence of magnetic field, then for a fixed field inclination θ the value of $F_\perp/F_o$ indeed depends only upon L/d and Q. This relation is shown in Fig. 2 for the field inclination ($\theta = 45^\circ$) giving maximum transverse thrust. Since the value of L/d is expected to be determined principally by geometric and mechanical considerations, it is seen that the determination of $F_\perp/F_o$ reduces to the determination of realistic values for the interaction parameter Q for rocket nozzle exhaust jets. This is described in succeeding sections.

III. THE ELECTRICAL CONDUCTIVITY OF SEEDED COMBUSTION GASES

The electrical conductivity, σ, which enters the expression for the interaction parameter Q is consequence of the presence of mobile charge carriers in the gas; i.e., the gas must be partially ionized to become a moderately good conductor. When the effects of electron-neutral (short range) collisions dominate those of the coulomb interactions (long range) between electrons and positive ions, the electrical conductivity of a partially ionized gas is simply related to the prevalent mole fraction X_e of electrons. Kinetic theory provides the useful result[3]

$$\sigma = 0.532 \frac{e^2}{(m_e\, kT)^{\frac{1}{2}}\, Q_\sigma} \cdot X_e \qquad (2)$$

where Q_σ is the effective electron-neutral collision cross-section, e and m_e are the charge and mass of the electron, respectively, and T is the gas temperature.†

In MKS units, if we introduce the numerical values

$$e = 1.6 \times 10^{-19} \text{ coulomb}$$
$$m_e = 0.911 \times 10^{-30} \text{ kg}$$
$$k = 1.38 \times 10^{-23} \text{ kg(meter)}^2\text{(sec)}^{-2}(^\circ\text{K})^{-1}$$

and express temperature in degrees Kelvin, then the units of electrical conductivity are mhos/meter. Thus the electrical conductivity can be estimated if the

† It will be assumed that the gas temperature and electron temperature are everywhere equal.

gas temperature, T, electron mole fraction X_e, and collision cross-section Q_σ are known. For the purposes of the present study, it will be assumed that the value of the electron-neutral cross-section, Q_σ, will not be very different from 10^{-19} (meter)^2 for most combustion gases[4] of interest and that this cross-section has no appreciable dependence on temperature level[5] (see Section VI, Part 5).

It will further be assumed that the condition of thermochemical equilibrium exists for the combustion gases at the nozzle inlet section. This means that the electron mole fraction X_e corresponding to chamber conditions is determined by thermodynamic considerations alone. Since the electrons present in the gas must originate from ionization of some of the molecules present in the chamber, it is clear that X_e will be large if an easily ionizable species is present in the product gases.

Table I shows values of the first ionization potential[6] for a selected group of atoms and molecules of interest in the present discussion. Also tabulated are the corresponding values of the energy change ΔE° across the ionization reaction (in kcal/mole)† and the corresponding "characteristic ionization temperature" $\Theta \equiv \Delta E^\circ/R$, where R is the universal gas constant (1.9872 cal/deg-mole). This temperature parameter is of physical interest since equilibrium statistical mechanics reveals that the extent of ionization will necessarily be small if the absolute gas temperature is small compared with Θ. Now, in rocket motor practice the chamber temperature levels are in the range of, say, 2000°K to 4000°K. But for the molecules which would be expected to prevail in ordinary combustion products (viz. H_2O, O_2, CO_2, CO, etc.) values of the characteristic temperature for ionization are in the range of 145,000°K to 167,000°K. By comparison, however, elements exist for which Θ is substantially lower. The class of elements having the lowest values of the characteristic ionization temperature, Θ, is the alkali group, with cesium displaying a Θ of only 44,900°K.

It can be verified a posteriori that the conclusion one is tempted to draw from this comparison is indeed valid, i.e., if one does not intentionally "seed" the usual products of combustion‡ with an easily ionizable substance, such as

---

†ΔE° (in kcal/mole) can be obtained from tabulated values of the ionization potential (in electron volts) by multiplication with 23.0631.

‡This may not be true for solid propellants containing metallic salts or metallic additives, such as aluminum.

TABLE I

DATA ON THE SINGLE IONIZATION OF SEVERAL ELEMENTS AND MOLECULES

Species	m	Ionization Energy Parameter		
		V,ev.	ΔE^o,Kcal/mole	Θ,^oK
Lithium	6.940	5.363	123.7	62,240
Sodium	22.991	5.12	118.	59,400
Potassium	39.100	4.318	99.59	50,110
Rubidium	85.48	4.159	95.92	48,270
Cesium	132.91	3.87	89.3	44,900
Aluminum	26.98	5.96	137.	69,200
Calcium	40.08	6.09	140.	70,700
Water Vapor	18.016	12.56	289.7	145,800
Oxygen (O_2)	32.000	12.5	288.	145,000
Carbon Dioxide	44.011	14.4	332.	167,000
Carbon Monoxide	28.011	14.1	325.	164,000
Ammonia	17.032	11.2	258.	130,000
Nitric Oxide	30.008	9.5	220.	110,000

potassium or cesium (or a compound thereof) then the electron mole fraction, and hence the electrical conductivity of the gas mixture, will be inconsequential (insofar as the present magnetogasdynamic application is concerned). Conversely, if one does "seed" with such a material the electrons which one will find in the gas will, overwhelmingly, be offspring of the seed material. In this simple case one can then calculate the electron mole fraction X_e by considering a single reversible reaction, written symbolically as

$$S \rightleftarrows S^+ + e \tag{3}$$

Now, in practice, only small amounts of the seed material S would be added to the combustion mixture to achieve the desired result.[7,8] If S is added with a mass† fraction, α_s, then the electron mole fraction‡ is found from the law of mass action to be proportional to the square root of α_s, i.e.

$$X_e = (K_p/p)^{\frac{1}{2}} (\mathfrak{m}_c/\mathfrak{m}_s)^{\frac{1}{2}} (\alpha_s)^{\frac{1}{2}} \tag{4}$$

where $K_p(T)$ is the equilibrium constant for the reaction (3) and the script $\mathfrak{m}$'s represent molecular weights. Combining Eqs. (2) and (4) with the assumption Q_σ = constant, we find the functional dependence

$$\sigma \propto p^{-\frac{1}{2}} T^{-\frac{1}{2}} [K_p(T)]^{\frac{1}{2}} \tag{5}$$

In this relation, the temperature dependence of the equilibrium constant can be obtained from the Saha equation of equilibrium statistical mechanics.[9,10] For the case of single ionization of alkali atoms†† the appropriate relation is

---

† This is much more convenient than the more commonly used mole fraction for specifying the seed concentration.

‡ subject to the assumption that the seed material does not undergo appreciable reaction with the combustion products

†† In this case the pre-exponential factor giving the dependence on electronic partition function ratios becomes approximately 1.00 in the temperature range of interest here. This factor has therefore been omitted from Eq. (6).

$$K_p(T) = (2\pi m_e)^{\frac{3}{2}} h^{-3} (kT)^{\frac{5}{2}} \exp(-\Theta/T) \tag{6}$$

where h is Planck's constant and all other quantities have already been defined. Therefore, subject to these approximations, the electrical conductivity, σ, of a seeded mixture of combustion gases will depend upon pressure and temperature in accord with the law[11]

$$\sigma \propto p^{-\frac{1}{2}} T^{\frac{3}{4}} \exp(-\tfrac{1}{2}\Theta/T) \tag{7}$$

This relation will be used to describe the variation in electrical conductivity for equilibrium isentropic nozzle expansions of seeded combustion gases.

Values of the equilibrium constant computed from Eq. (6) are given in Table II for the useful range of temperatures and Θ/T. Using Table II, one can rapidly evaluate the equilibrium constant K_p for any chamber temperature and seed material (i.e., any Θ). The electron mole fraction is then evaluated from Eq. (4) and inserted into the electrical conductivity relation (2). It is seen that the absolute value of conductivity at the nozzle inlet section is therefore determinable from a knowledge of the gas pressure, p_c, temperature, T_c, and mean molecular weight, $\mathfrak{M}_c$, together with the nature of the seed material (Θ, $\mathfrak{M}_s$) and the fractional extent of seeding (α_s). If equilibrium were maintained during the nozzle expansion the electrical conductivity would vary in accord with Eq. (7), since the mole fraction X_s of ionizable material would be sensibly constant. Moreover, the seed material may often be regarded as being immersed in a carrier gas which expands isentropically through the nozzle. Then, if the chemical composition of this carrier gas does not change,† pressure and temperature in the nozzle will be related in accord with[12]

$$\frac{p}{p_c} = \left(\frac{T}{T_c}\right)^{\frac{\gamma}{\gamma-1}} \tag{8}$$

It follows that if ionization equilibrium were maintained everywhere, then for a prescribed value of the specific heat ratio, γ, the conductivity ratio σ/σ_c

†i.e., if the expansion process is chemically frozen

TABLE II

VALUES OF - LOG_{10} K_p FOR THE SINGLE IONIZATION OF ALKALI ATOMS

T °K	Θ/T_c				
	0	10	20	30	40
1000	-1.0172	3.3257	7.6686	12.0116	16.3545
1500	-1.4575	2.8855	7.2284	11.5714	15.9143
2000	-1.7698	2.5731	6.9161	11.2590	15.6020
2500	-2.0121	2.3308	6.6738	11.0167	15.3597
3000	-2.2101	2.1329	6.4758	10.8188	15.1617
3500	-2.3774	1.9655	6.3085	10.6514	14.9944
4000	-2.5224	1.8205	6.1635	10.5064	14.8494
4500	-2.6503	1.6927	6.0356	10.3786	14.7215
5000	-2.7647	1.5783	5.9212	10.2642	14.6071

would be a function only of the pressure ratio p_c/p (say) and the parameter Θ/T_c. In connection with a subsequent nozzle flow recombination study, this conductivity ratio function will be shown graphically in Figs. 4, 5 and 6, for a carrier gas specific heat ratio of 1.2. The values of σ/σ_c can now be brought to bear on the determination of the magnetogasdynamic interaction parameter Q for the exhaust section of rocket motors.

IV. ANTICIPATED VALUES OF THE MAGNETOGASDYNAMIC INTERACTION PARAMETER Q

While we are interested in the value of the magnetogasdynamic interaction parameter Q at the nozzle exit section, a cursory study of the rocket motor literature[13,14,15] reveals that most information for various propellant combinations is tabulated at chamber conditions. Thus for prescribed chamber pressures (usually 300 psia, or 1000 psia) extensive data is available giving mean molecular weight, chamber temperature, ratio of specific heats, characteristic velocity (c*) and sometimes detailed species concentrations. This abundance of chamber data suggests that for design purposes it will be convenient to split the determination of the interaction parameter Q at the nozzle exit section into several more or less independent factors:

(a) dependence on particular propellant/additive system
(b) dependence on chemical kinetic parameters governing departures from ionization equilibrium†
(c) dependence on available magnetic field strength
(d) dependence on physical scale (thrust level) other than that due to (b)
(e) dependence on expansion conditions (pressure ratio across nozzle)

This can be accomplished by rewriting Eq. (1) as follows

---

† Throughout this work the term nonequilibrium deals with the inability of the electron-ion recombination rate to maintain equilibrium in an expanding flow. This should be distinguished from the use of the phrase nonequilibrium ionization to describe such phenomena as chemi-ionization.[26]

$$Q = Q_{ref}\left(\frac{\sigma_{ex}}{\sigma_{ex,eq}}\right)\left(\frac{B}{B_{ref}}\right)^2\left(\frac{d_t}{d_{ref}}\right)\left\{\left(\frac{\sigma_{ex}}{\sigma_c}\right)_{eq}\left(\frac{\rho_c}{\rho_{ex}}\right)\left(\frac{A_{ex}}{A_t}\right)^{\frac{1}{2}}\left(\frac{c^*}{c}\right)\right\} \qquad (9)$$

where

$$Q_{ref} \equiv \frac{\sigma_c B_{ref}^2 d_{ref}}{\rho_c c^*} \qquad (10)$$

and c* is the characteristic velocity of the propellant. The factors in this decomposition have the following significance:

(a) Q_{ref} fixes the <u>level</u> of the magnetogasdynamic parameter for some reference motor size d_{ref} and field strength B_{ref} and is computed based on <u>chamber</u> conditions. As will be seen, Q_{ref} can be calculated for each propellant system for which theoretical performance, <u>chamber</u> temperature, and molecular weight data are available and will depend upon the nature and amount of the "seed" material added to enhance the electrical conductivity. In the MKS system of units convenient choices for B_{ref} and d_{ref} might be 1 weber/meter^2 and 1 meter, respectively. Numerical values for Q_{ref} in practical cases will be given later on.

(b) The factor $\sigma_{ex}/\sigma_{ex,eq}$ represents the enhancement in the conductivity at the exhaust section which would result from the inability of ion-electron recombination rates to keep pace with the rapidly changing pressure-temperature environment in the nozzle.[16,17] This enhancement will be discussed in some detail in Part 2 of this section, as well as Appendix B.

(c) The factor $(B/B_{ref})^2$ accounts for the effect on the interaction parameter Q of field strength capabilities differing from B_{ref}.

(d) The factor d_t/d_{ref}, being the ratio of the actual throat diameter to d_{ref}, accounts for the effect on Q of the <u>scale</u> of the motor in question. As will be seen in Part 3 of this section d_t/d_{ref} is proportional to the square root of the thrust level for a given chamber pressure. Scale effects are also implicit in part (b) above, but these require separate treatment.

(e) In Eq. (9) the factor in brackets, <u>i.e.</u>

$$E \equiv \frac{\bar{\sigma}_{eq}\,\bar{A}^{\frac{1}{2}}}{\bar{\rho}\,\bar{u}} \qquad (11)$$

is a function of only 3 variables: Θ/T_c, specific heat ratio, γ, and expansion pressure ratio, p_c/p. It is precisely that function by which $Q_{ref}(\sigma_{ex}/\sigma_{ex,eq})(B/B_{ref})^2(d_t/d_{ref})$ must be multiplied to recover $Q \equiv \sigma_{ex}B^2\, d/(\rho_{ex}\, c)$. Discussion of this "equilibrium expansion factor", E, will be postponed to Part 4 of this section.

On the basis of this decomposition it becomes possible to combine calculations of Q_{ref} for all of the usual propellant combinations with data read from a few universal graphs to arrive at the value of the interaction parameter Q, expected in the jet exhaust for any desired expansion ratio, seed material and concentration, magnetic field strength and physical scale. A knowledge of Q and the effective field length (measured in jet diameters) is then all that is needed to determine the control force (Fig. 2).

1. Establishment of the Reference Value, Q_{ref}, of the Magnetogasdynamic Interaction Parameter

Since it will be seen that it is easy to correct the results of calculations of Q_{ref} for the effects of changing either the seed material or the seed mass fraction, numerical results will be given here for a class of rocket motors operating with chamber pressures of 300 psia and 1000 psia, respectively, seeded with cesium to the extent of one percent by mass. For this case: $\Theta = 44{,}900^{\circ}K$, $\alpha_s = 10^{-2}$ and $m_s = 132.91$. Reference quantities are $d_{ref} = 1$ meter and $B_{ref} = 1$ Weber/meter^2 = 10,000 gauss. Numerical results for seven fuel/oxidizer combinations at 300 psia chamber pressure[13,18,19] are collected in Table III. Results for 14 fuel/oxidizer combinations at 1000 psia chamber pressure[15,20] are collected in Table IV.

In considering the numerical values of Q_{ref} tabulated here, it is found that they correlate almost solely with chamber temperature. This indicates that differences in m_c and γ from propellant to propellant are dominated by the exponential dependence of electrical conductivity on chamber temperature (see Eq. (7)). This correlation is shown in Fig. 3, where Q_{ref} is plotted vs. chamber temperature (on log-log paper) and the individual points are identified with the propellants appearing in Table III. This means that to a good approximation

$$Q_{ref} \propto T_c^{\frac{5}{4}} \exp\left(-\tfrac{1}{2}\Theta/T_c\right) \qquad (12)$$

TABLE III

ROCKET MOTOR DATA† FOR CHAMBERS‡ OPERATING AT 300 PSIA

Propellants	O/F Ratio	Q_{ref}	T_c	c*	c	γ_c
Lox-Ammonia††	1.4	1.5×10^{-2}	3010	1770	2500	1.23
Lox-Gasolene	2.5	3.5×10^{-2}	3295	1690	2370	1.22
Lox-Hydrazine	0.5	0.71×10^{-2}	2750	1845	2542	1.23
Lox-Kerosene	2.2	4.0×10^{-2}	3350	1737	2428	1.24
Flourine-Hydrazine	1.9	$30. \times 10^{-2}$	4430	2106	2928	1.33
N_2O_4-Hydrazine	1.0	1.5×10^{-2}	2975	1734	2420	1.27
Hydrogen	7.937	4.7×10^{-2}	3437	2077	2920	1.20

TABLE III (CONTINUED)

Propellants	$\mathfrak{M}_c$	$X_{e,c}$	σ_c	$n_{e,c}$	Reference
Lox-Ammonia††	19.7	0.63×10^{-4}	4.4×10^{1}	3.1×10^{15}	13
Lox-Gasolene	22.7	1.49×10^{-4}	1.0×10^{3}	0.68×10^{16}	13
Lox-Hydrazine	15.9	2.58×10^{-5}	1.9×10^{1}	1.4×10^{15}	13
Lox-Kerosene	21.6	1.67×10^{-4}	1.1×10^{2}	0.74×10^{16}	13
Flourine-Hydrazine	18.0	1.10×10^{-3}	0.63×10^{3}	3.7×10^{16}	13
N_2O_4-Hydrazine	18.8	0.58×10^{-4}	4.1×10^{1}	2.9×10^{15}	13
Hydrogen-Oxygen	15.7	1.70×10^{-4}	1.1×10^{2}	0.74×10^{16}	19

† Units are as follows: T_c in °K; c* in meter $(sec)^{-1}$; γ_c dimensionless; $\mathfrak{M}_c$ in gm $(gm\text{-}mole)^{-1}$; X_e dimensionless; σ_c in mho $(meter)^{-1}$; n_e in electrons $(cm)^{-3}$, c in meter $(sec)^{-1}$

‡ Seeded with 1 percent cesium (by mass); $d_{ref} \equiv 1$ meter; $B_{ref} \equiv 1$ Weber $(meter)^{-2}$

†† Lox ≡ liquid oxygen

TABLE IV

ROCKET MOTOR DATA FOR CHAMBERS OPERATING AT 1000 PSIA†

Propellants	O/F Ratio	Q_{ref}	T_c	c*	c	γ_c	$\mathfrak{M}_c$	$X_{e,c}$	σ_c	$n_{e,c}$	Reference
Lox-Ammonia	1.30	2.0×10^{-2}	3044	1763	2795	1.22	19.10	2.59×10^{-4}	1.80×10^{2}	0.424×10^{17}	31
Lox-RP1	2.20	6.0×10^{-2}	3541	1778	2804	1.24	21.6	$.830 \times 10^{-3}$	5.38×10^{2}	1.17×10^{17}	31
Lox-Hydrazine	0.74	3.9×10^{-2}	3275	1873	2952	1.24	18.0	4.93×10^{-4}	3.32×10^{2}	0.752×10^{17}	31
Lox-Hydrogen	3.46	1.6×10^{-2}	2736	2429	3805	1.26	8.8	1.45×10^{-4}	1.07×10^{2}	0.265×10^{17}	31
Flourine-Hydrazine	1.85	3.8×10^{-1}	4508	2128	3275	1.32	18.4	4.74×10^{-3}	2.72×10^{3}	5.25×10^{17}	31
Flourine-Hydrogen	4.60	5.0×10^{-2}	3091	2536	3903	1.33	8.8	4.34×10^{-4}	3.01×10^{2}	0.702×10^{17}	31
RFNA-Hydrogen	5.55	3.9×10^{-3}	2422	2036	3187	1.26	11.13	3.85×10^{-5}	3.01×10^{1}	0.0793×10^{17}	31
RFNA-UMDH	2.45	2.1×10^{-2}	3122	1661	2628	1.23	22.0	2.99×10^{-4}	2.06×10^{2}	0.479×10^{17}	31
N_2O_4-Hydrazine	1.10	2.2×10^{-2}	3091	1754	2775	1.23	19.5	2.92×10^{-4}	2.03×10^{2}	0.472×10^{17}	31
N_2O_4-Hydrogen	4.90	$.63 \times 10^{-2}$	2525	2131	3324	1.27	10.5	$.606 \times 10^{-4}$	4.64×10^{1}	0.120×10^{17}	31
TFH-Hydrogen	6.50	2.9×10^{-2}	2966	2254	3461	1.34	10.7	2.77×10^{-4}	1.96×10^{2}	0.466×10^{17}	31
TFH-UMDH	3.00	1.4×10^{-1}	3983	1844	2873	1.28	22.13	1.92×10^{-3}	1.17×10^{3}	2.40×10^{17}	31
Ammonium Perchlorate	80/20	$.83 \times 10^{-2}$	2840	1488	2368	1.23	24.6	1.23×10^{-4}	$.889 \times 10^{2}$	0.216×10^{17}	15
Aluminized Perchlorate	68/17/15‡	$.59 \times 10^{-1}$	3519	1791	2803	1.26	20.9	$.804 \times 10^{-3}$	5.22×10^{2}	1.14×10^{17}	15

† Footnotes of Table III apply to this table as well. ‡Numbers represent, respectively, the percentages of NH_4ClO_4, Binder (gross formula = $C_{23}H_{28}O_4$) and aluminum.

and new values of Q_{ref} (at the same chamber pressure) can be estimated simply from a knowledge of the chamber temperature alone, and any value of Q_{ref} already given here.

It is also relatively simple to take the values of Q_{ref} computed for cesium seeding and convert them to apply to other seeding materials, since we have already seen that if the seed mass fraction, α_s, is preserved

$$Q_{ref} \propto (m_s)^{-\frac{1}{2}} \exp\left(-\tfrac{1}{2}\Theta/T_c\right) \tag{13}$$

Thus, if we have two seed materials, designated by the subscripts 1 and 2, the value of Q_{ref} will change in accord with

$$\frac{Q_{ref,1}}{Q_{ref,2}} = \left(\frac{m_2}{m_1}\right)^{\frac{1}{2}} \exp\left(-\frac{\Delta\Theta}{2T_c}\right) \tag{14}$$

where $\Delta\Theta \equiv \Theta_1 - \Theta_2$.

Corrections to account for smaller (and perhaps more realistic[7]) seed mass fractions are likewise made with the use of the square root relation $Q_{ref} \propto (\alpha_s)^{\frac{1}{2}}$. Thus, values for a tenth of a percent (by mass) cesium seed would be smaller than the values given in Tables III and IV by $1/\sqrt{10} = .3162$. In practice, an optimum seed concentration will probably exist, as has been described by Rosa[7] and Sherman.[8]

2. Enhancement of the Interaction Parameter Due to Electron-Ion Recombination Lags in the Nozzle

The nonequilibrium effect is intrinsically the most difficult to assess with any generality; however, some progress can be made by drawing on the work of Bray,[21] Hall,[22] *et.al.* on deviations from dissociation equilibrium in hypersonic nozzle expansions, as well as that of Smith,[16] and Eschenroeder and Daiber.[17] In principle, for a nozzle of a prescribed shape, a weak coupling (between the ion species and the carrier gas) approximation allows the history of the reaction to be readily obtained from a consideration of the conservation equation for electrons alone. This equation will contain a convective term (see

Eq. B-6) and a recombination (chemical kinetic) term.† The latter is expected to take the nonlinear form (see Eq. B-5)

$$\dot{w}_e = - \alpha_r m_e[(n_e)^2 - (n_{e,eq})^2] \tag{15}$$

where $\dot{w}_e$ is the net mass rate of production of electrons per unit volume. Here α_r is, formally, the ion recombination coefficient. Actually, the dominant electron loss mechanism need not be "bimolecular" so that, in general, the ion recombination coefficient appearing in Eq. (15) can have a dependence upon total pressure as well as temperature. This is usually expressed by a power law of the form

$$\alpha_r \propto T^{\omega_T} p^{\omega_p} \tag{16}$$

where the appropriate set of exponents (ω_T, ω_p) depends upon the anticipated microscopic mechanism. As described in Appendix B, three possible sets of values are given in Table V. Because of the extensive variation of temperature, and particularly pressure in a nozzle flow, predictions of electron recombination lags using each of the models above differ considerably, as will be seen.

Our approach to this problem has been to consider a family of realistic nozzle shapes and to write a nondimensional differential equation satisfied by the electrical conductivity itself.‡ To obtain a body of approximate results for immediate use, we have invoked the observations of Bray and Hall, _etal_., that the mole fraction of "relaxing" species is likely to suddenly "freeze" out to an asymptotic value somewhere in the nozzle, it is possible to make a rough estimate of the conductivity, σ_f, of the gas at the freeze point. In accord with Eq. (2), the electrical conductivity, σ_{ex}, to be expected at the nozzle exit will then be given by

$$\sigma_{ex} = \sigma_f \cdot (T_f/T_{ex})^{\frac{1}{2}} \tag{17}$$

---

†axial diffusion is neglected

‡For radar attenuation and related problems, the electron number density is of more direct interest. This information can easily be recovered from the results given in this report by everywhere making the replacement $\bar{\sigma}\sqrt{\bar{T}} \rightarrow \bar{X}_e$ and noting that $\bar{X}_e = \bar{n}_e \bar{T}/\bar{p}$. Therefore $\bar{n}_e = \bar{p}\,\bar{\sigma}/\sqrt{\bar{T}}$.

TABLE V

TEMPERATURE AND PRESSURE DEPENDENCE
OF THE ION RECOMBINATION COEFFICIENT[23,24,25]
(ABRIDGED)†

ω_T	ω_p	Mechanism
$-\frac{7}{2}$	1	Three Body, Thompson (1924)
$+\frac{1}{2}$	-1	Three Body, Langevin (1903)
$-\frac{3}{2}$	0	Dissociative, Bates (1950)

†See Table VII for more detail.

provided the temperature dependence of the cross-section Q_σ is neglected.

Within a given class of nozzles, if the values of the following parameters are prescribed: specific heat ratio γ of the carrier gas, the exponents ω_T and ω_p, and Θ/T_c; then exit value of the nondimensional electrical conductivity σ_{ex}/σ_c will depend only on the magnitude of a nondimensional <u>recombination parameter</u>

$$C_r \equiv \frac{\alpha_{r,c}\, n_{e,c}\, d_t}{c^*} \tag{18}$$

This parameter can be interpreted physically as the ratio of the characteristic flow time d_t/c^* to the electron half life $(\alpha_{r,c}\, n_{e,c})^{-1}$ in the chamber. A discussion of the magnitudes of C_r likely to be obtained in practice will be postponed to Section V. It can be verified from the previous relations that the recombination parameter C_r will scale with pressure and temperature approximately as

$$C_r \propto p^{\omega_p + \frac{1}{2}}\, T^{\omega_T - \frac{1}{4}} \exp\left(-\tfrac{1}{2}\Theta/T\right) \tag{19}$$

for a fixed fractional seed concentration.

We present here the results of the approximate "sudden freeze" analysis given in detail in Appendix B.† The accuracy of this method is also discussed in Appendix B, by comparing its results with those of an exact solution. The results given here are presented as contours of constant recombination parameter C_r on the map of conductivity ratio vs. pressure ratio for isentropic expansions (see Figs. 4,5,6). The carrier gas is assumed to have a specific heat ratio of $\gamma = 1.2$ in each case. Thus the only difference between Figs. 4, 5 and 6 is in the choice of the exponents ω_T and ω_p, describing the dependence of the ion recombination coefficient α_r on temperature and pressure. Fig. 6 corresponds to one extreme choice [$\omega_T = -7/2$, $\omega_p = +1$ (Three-body,Thompson)], whereas Fig. 4 corresponds to another extreme choice [<u>viz</u>. $\omega_T = +\frac{1}{2}$, $\omega_p = -1$ (Three-body,Langevin)]. Fig. 5, corresponding to $\omega_T = -3/2$, $\omega_p = 0$ (Dissociative, Bates) displays behavior intermediate between those of Fig. 4 and 6, as expected. Also shown on each of these maps is a small triangle, the hypotenuse of which defines contours (straight lines

†An improved approximate method based on somewhat different arguments is also discussed in Appendix B.

on log-log paper†) of constant electron mole fraction. As will be shown, a knowledge of this straight line slope allows the variation of electrical conductivity in the frozen section to be followed graphically (see Eq. (17)) until the exit section is reached. All of the results given here pertain to a particular family of axisymmetric nozzle shapes (frustum of cone tangent to inside of torus as shown in meridional view in Fig. 7) considered to be a fair representation of those often used in rocket motor practice. The divergence half angle of the conical section was assumed to be 15° and the radius of curvature at the throat was taken to be equal to the throat diameter.

Figs. 4, 5 and 6 can therefore be used to estimate whether, in practice, the recombination parameter C_r is small enough to cause significant deviations from ionization equilibrium within the nozzle and, if so, what the effect on the electrical conductivity at the exit section is likely to be. The graphical procedure is illustrated schematically in Fig. 8. If freezing indeed occurs within the nozzle for the desired pressure ratio and estimated recombination parameter, then the appropriate equilibrium line is followed to the point where it intersects the contour of constant C_r. Thereafter, one follows the contour† of constant electron mole fraction which passes through this point until the desired pressure ratio is reached. The enhancement ratio, $\sigma_{ex}/\sigma_{ex,eq}$, due to ionization nonequilibrium, is then calculated from the ratio, σ_{ex}/σ_c, so obtained to the value $\sigma_{ex,eq}/\sigma_c$, obtained by simply following the equilibrium line down to the desired pressure ratio.

3. Effect of Physical Size (or Thrust Level) on the Magnitude of the Magnetogasdynamic Interaction Parameter

Quite apart from the scale effect introduced by ionization nonequilibrium phenomena, the effect of physical scale on the anticipated value of the magnetogasdynamic interaction parameter Q at the nozzle exit is explicitly represented by the presence of the ratio d_t/d_{ref} in Eq. (9). If F_o is the thrust level of the

---

†When the electron mole fraction is constant, Eqs. (17) and (8) combine to give $d[\ln \bar{\sigma}]/d[\ln(1/\bar{p})] = \frac{1}{2}[(\gamma - 1)/\gamma]$. Thus, contours of constant electron mole fraction are straight lines whose slope is the same everywhere on the $\log \bar{\sigma}$ - $\log (1/\bar{p})$ plane, as indicated by the triangles shown in Figs. 4, 5 and 6.

motor in question (expressed in pounds) and p_c is the chamber pressure in psia, then (in accord with our previous choice $d_{ref} = 1$ meter) a convenient relation for d_t/d_{ref} is

$$\frac{d_t}{d_{ref}} = 2.54 \times 10^{-2} \left(\frac{4}{\pi}\right)^{\frac{1}{2}} \left(\frac{c^*}{c}\right)^{\frac{1}{2}} \left(\frac{F_o}{p_c}\right)^{\frac{1}{2}} \tag{20}$$

<u>i.e.,</u> for a fixed propellant combination, chamber pressure and expansion ratio we have the square root dependence: $d_t/d_{ref} \propto (F_o)^{\frac{1}{2}}$.

It should be remarked that while values of Q_{ref} in effect compare directly to motors of the <u>same geometric size</u>, the sequence should not be noticeably altered if the comparison were made for motors of <u>equal thrust</u> at the same chamber pressure level. This is a consequence of the fact that $(c^*/c)^{\frac{1}{2}}$ exhibits only a very slight variation in going from one propellant combination to the next. For example, $(c^*/c)^{\frac{1}{2}}$ only varies by 1.2 percent for the first six propellant combinations listed in Table III.

4. <u>Effect of Nozzle Expansion Conditions on the Magnitude of the Magnetogasdynamic Interaction Parameter at the Nozzle Exit Section</u>

It has already been shown that the value of the interaction parameter Q at the nozzle exit section can be computed from

$$Q = Q_{ref} \left(\frac{\sigma_{ex}}{\sigma_{ex,eq}}\right) \left(\frac{B}{B_{ref}}\right)^2 \left(\frac{d_t}{d_{ref}}\right) E \tag{9}$$

where

$$E(p_c/p_{ex};\ \Theta/T_c, \gamma) \equiv \left(\frac{\sigma_{ex}}{\sigma_c}\right)_{eq} \left(\frac{\rho_c}{\rho_{ex}}\right) \left(\frac{A_{ex}}{A_t}\right)^{\frac{1}{2}} \left(\frac{c^*}{c_{ex}}\right) \tag{11}$$

Thus, the function E may be considered to account for all of the remaining effects of the gasdynamic conditions of expansion on the level of the interaction parameter Q. This composite expansion factor has been plotted once and for all for two values of the specific heat ratio $\gamma \equiv c_p/c_v$ ($\gamma = 1.20$ and 1.30) and several values of the ionization parameter Θ/T_c covering the pressure ratio range of practical interest. Results are presented in Figs. 9 and 10.

V. NUMERICAL EXAMPLE: TRANSVERSE THRUST FOR A 300 PSIA CHAMBER PRESSURE, 10,000 POUND THRUST OXYHYDROGEN MOTOR; 0.1% POTASSIUM SEED

The use of the graphs and tables already presented may best be described with the help of a numerical example. With this in mind, we consider the combustion chamber specified above (in the section title) and take the ambient pressure to be one atmosphere.

1. Determination of $\dot{Q}_{ref}$

For a one percent cesium seed Q_{ref} is obtained from Table III as 4.7×10^{-2}. For a tenth of a percent cesium seed the result would be $4.7 \times 10^{-2}/\sqrt{10}$ or 1.5×10^{-2} (see Eq. (4)). To convert this result to potassium, we make use of Eq. (14) noting that $\Theta_K - \Theta_{Cs} = 50{,}110 - 44{,}900 = 5210^{\circ}K$ (Table I), $T_c = 3437^{\circ}K$ (Table III) and $m_{Cs}/m_K = 132.91/39.10 = 3.4$ (Table I). Therefore

$$Q_{ref,K} = Q_{ref,Cs} \cdot \sqrt{3.4}\, \exp[-\tfrac{1}{2}(5210)/(3437)]$$

or

$$Q_{ref,K} = 1.3 \times 10^{-2}$$

2. Effect of Electron-Ion Recombination Lag (This discussion is best postponed until after Part 5)

3. Effect of Magnetic Field Strength

Let us assume that a magnetic field strength of 3 Weber/meter^2 is available. Then $(B/B_{ref})^2 = (3/1)^2 = 9$ (see Eq. (9)).

4. Effect of Physical Scale (or Thrust Level)

From Table III we find $c^* = 2077$ meter $(sec)^{-1}$ and $c = 2920$ meter $(sec)^{-1}$. Therefore, since the thrust level F_o is 10,000 lbs. and $p_c = 300$ psia, Eq. (20) gives

$$\frac{d_t}{d_{ref}} = 2.54 \times 10^{-2} \left(\frac{4}{\pi}\right)^{\frac{1}{2}} \left(\frac{2077}{2920}\right)^{\frac{1}{2}} \left(\frac{10{,}000}{300}\right)^{\frac{1}{2}} = 0.140$$

5. Determination of the Equilibrium Expansion Factor, E

The determination of E involves a knowledge of Θ/T_c, the specific heat ratio, γ, and the pressure ratio p_c/p. For potassium $\Theta = 50{,}110^{\circ}K$ (Table I), so that $\Theta/T_c = 50{,}110/3437 = 14.6$. The pressure ratio is given by $300/14.7 = 20.4$ (i.e., the chamber pressure expressed in atmospheres). Table III also gives $\gamma \equiv c_p/c_v$ as 1.2, so that Fig. 9 is appropriate. Introducing these values, one finds $E = 0.44$. With the exception of the nonequilibrium effect, these values of Q_{ref}, $(B/B_{ref})^2$, d_t/d_{ref} and E allow an estimate to be made of the interaction parameter Q to be expected at the nozzle exit section. Since $\sigma_{ex}/\sigma_{ex,eq} \geqslant 1$ we can then immediately state the result

$$Q \geqslant Q_{ref}\ (B/B_{ref})^2\ (d_t/d_{ref})\ E$$

or

$$Q \geqslant (1.3 \times 10^{-2})(9)(0.140)(0.44) = 0.72 \times 10^{-2}$$

The extent to which nonequilibrium ionization will increase the actual value of the interaction parameter Q above its minimum value of 0.72×10^{-2} will now be considered in the light of the analysis of Appendix B.

2. (Continued) Effect of Electron-Ion Recombination Lag

To assess the importance of electron-ion recombination lag it is necessary to estimate the most important electron loss mechanism[26] and, on the basis of this mechanism, evaluate the most probable value of the recombination parameter C_r defined by Eq. (18). Before doing this, however, it can be verified that for a given chamber pressure, seed material and concentration, small values of C_r will be favored by propellant combinations with low values of the characteristic velocity c*. This is because the effect of reduced chamber temperature on the electron number density $n_{e,c}$ in the chamber outweighs the effect of temperature on the recombination coefficient $\alpha_{r,c}$ or the direct effect of reduced c* on C_r. It is also clear that small values of the recombination parameter C_r will be favored by small (throat diameter) motors. What is least clear, unfortunately, is the establishment of the most probable value of the recombination coefficient $(\alpha_{r,c})$ in the chamber, and the law governing its temperature and pressure variation (i.e., the coefficients ω_p and ω_T).

The solid curve shown in Fig. 11 gives the pressure dependence of the ion recombination coefficient for air at ambient temperature.† The curve may be seen to have two distinct branches separated by a transition region. The low pressure branch, labeled Thompson, 300°K, is believed to scale according to $T^{-7/2}$, whereas the high pressure branch labeled Langevin, 300°K, is believed to scale according to $T^{1/2}$. The displaced lines marked 3000°K then represent the corresponding branch positions at a temperature level more representative of rocket motor practice. If the $\alpha_r(p;T)$ curves for other gases retain this same shape at elevated temperatures, then the Thompson coefficient should prevail at rocket motor pressures and this value would be considerably smaller than the value obtained by extrapolating the Langevin branch. Moreover, since pressure and temperature will be related as in Eq. (8), the Thompson branch should prevail throughout the nozzle. This is illustrated by the locus of recombination coefficients $\alpha_r(p)$, superimposed on Fig. 11, and calculated for isentropic expansion from a 300 psia, 3000°K chamber with $\gamma = 1.2$. The implication is that, of the sets of coefficients ω_T, ω_p introduced earlier, the set which gives rise to the earliest departures from equilibrium is indeed applicable throughout the nozzle. It can therefore be said that predictions based on the Thompson mechanism, by giving the smallest absolute estimates of the recombination rate parameter C_r and the largest anticipated departures from equilibrium (compare Figs. 4,5,6), represent the most optimistic case for magnetogasdynamic applications, i.e., lead to the largest expected values of the nonequilibrium enhancement $\sigma_{ex}/\sigma_{ex,eq}$. Returning to the particular numerical example treated in this section, it can now be shown that even in the most optimistic case no significant nonequilibrium enhancement of the electrical conductivity at the exit section should be expected. This can be demonstrated as follows.

The reference electron number density $n_{e,c}$ given in Table III is 0.74×10^{16} electrons/cm^3. When corrected for 0.1% potassium seed, this becomes about 2×10^{15} electrons/cm^3. The recombination coefficient, $\alpha_{r,c}$, under these pressure-temperature conditions is expected to be of the order of 10^{-8} cm^3(sec)$^{-1}$ (see Fig. 11). Therefore, the characteristic time for electron decay will be $\tau_{chem} = (\alpha_{r,c}\, n_{e,c})^{-1} \simeq 5 \times 10^{-8}$ sec. On the other hand, the characteristic flow time $\tau_{flow} = d_t/c^*$ is found to be $0.140/2077 = 0.67 \times 10^{-4}$ sec. Therefore, the recombination parameter, $C_r \equiv \tau_{flow}/\tau_{chem}$, will be of the order of 1.3×10^3. Consulting

†This graph is extracted from Fig. 77, p. 135 of Von Engel[23], and strictly applies to air at room temperature (see Appendix B).

Fig. 6, we notice that such a contour would cross the (interpolated) equilibrium curve corresponding to $\Theta/T_c = 14.6$ at a value of p_c/p approximately equal to 18.5 (i.e., fairly near the exit section value of 20.4). Therefore, even in the most optimistic case for this numerical example, departures from ionization equilibrium at the nozzle exit section are expected to be small, being of the order of only 16 percent. We conclude that to within the accuracy of the present analysis, the inequality sign appearing in the earlier statement: $Q \gtrsim 0.72 \times 10^{-2}$ could be removed. At best we may take $Q = 0.84 \times 10^{-2}$.

It is now possible to estimate the magnetogasdynamic control force $F_\perp$ that would result from the application of a 30,000 gauss (3 Weber/meter^2) magnetic field (inclined at 45°) to the exhaust jet. If the axial extent of the field is comparable to the jet diameter, then $L/d \simeq 1$ and $F_\perp/F_o$ is found from Eq. (A18) of Appendix A, to be approximately† $\frac{1}{2} Q = 4.2 \times 10^{-3}$. Thus 0.42 percent of the gross thrust would be available for control purposes. Since the undisturbed thrust level, F_o, is 10,000 pounds, the anticipated control force, $F_\perp$, would then be approximately 42 pounds for this case. A field strength of 100,000 gauss (10 Weber/meter^2) would increase this value to $(10/3)^2 \cdot (42)$ or about 470 pounds, i.e. slightly less than 5 percent of the gross thrust of the engine.

VI. DISCUSSION

An examination of the equations and figures presented in previous sections allows some general conclusions to be drawn about the effects of various parameters on the anticipated magnetogasdynamic control force. While it is quite obvious that large magnetic field strengths are desirable, the effects of such parameters as physical scale, chamber pressure, specific heat ratio etc., are not quite so evident, particularly when the possibility of nonequilibrium ionization at the exit section is allowed for. In accord with the previous formulation, the individual influence of these parameters (other than field strength) on the interaction parameter Q can be discussed by forming the ratio

$$\frac{Q'}{Q} = \frac{Q_{ref}'}{Q_{ref}} \cdot \frac{d_t'}{d_t} \cdot \frac{E'}{E} \cdot \frac{(\sigma_{ex}/\sigma_{ex,eq})'}{(\sigma_{ex}/\sigma_{ex,eq})} \qquad (21)$$

† If Q had exceeded 10^{-2} the use of Fig. 2 would be more convenient.

where the primed variables may be taken to represent values of the individual quantities after a particular parameter (say, Θ/T_c, γ, p_c/p_{ex}, d_t/d_{ref}) has been changed. Since the control forces are monotonic in the interaction parameter Q, any factor which (all things considered) causes Q' to exceed Q would be expected, in practice, to favor larger MHD control forces.

1. Effect of Θ/T_c on Interaction Parameter

It is appropriate that the effect of this parameter be discussed first since it is found to dominate all others. Indeed, a consideration of its magnitude accounts for the effect of the remaining parameters on the interaction parameter Q.

If the only difference between two rocket motors was the value of the characteristic ionization temperature Θ corresponding to the seed material, then the values of Q_{ref}, E and $\sigma_{ex}/\sigma_{ex,eq}$ would likewise be different. Q_{ref} and E would be larger for the low Θ seed material motor since Eq. (12) shows that $Q_{ref} \propto \exp(-\frac{1}{2}\Theta/T_c)$, while Figs. 9 and 10 reflect the strong effect of Θ/T_c on the factor $(\sigma_{ex}/\sigma_c)_{eq}$ appearing in the equation for E. However, it cannot be concluded that Q would be larger until the nonequilibrium factor $(\sigma_{ex}/\sigma_{ex,eq})$ is investigated. This is particularly true since low values of Θ tend to increase the magnitude of the recombination parameter C_r, thereby suggesting smaller departures from equilibrium. In addition, the value of the normalized equilibrium electrical conductivity $(\sigma_{ex}/\sigma_c)_{eq}$ will be larger, which also suggests smaller values of the nonequilibrium enhancement $\sigma_{ex}/\sigma_{ex,eq}$. When these factors are combined, however, it is found that the equilibrium benefits of low characteristic temperature Θ more than compensate for the nonequilibrium gains associated with larger values of Θ for the parameter range likely to be of interest in chemical propulsion. Thus, even in the nonequilibrium regime it would appear to be advantageous to use the seed material with the lowest possible ionization potential.

2. Effect of Specific Heat Ratio

For motors in which equilibrium ionization is likely to be maintained throughout the nozzle, the strong effect of specific heat ratio which shows up in Figs. 9 and 10 can be traced to the steep temperature dependence of the electrical conductivity for realistic values of the parameter Θ/T_c. To illustrate this

point, let us consider the effective value of the exponent n in the power law[27]

$$\sigma \propto T^n \tag{22}$$

assuming that cesium (i.e., the element having the lowest available value of Θ) is used as the seed material. For the purpose of comparing effective values of n likely to be realized in rocket motor practice, it is convenient to consider a temperature (drop) ratio which is characteristic of each propellant gas combination, say $2/(\gamma + 1)$, which will be recognized at the ratio of the throat temperature to the chamber temperature for an isentropic expansion. This temperature drop, if unaccompanied by a partially compensating pressure drop, would give rise to values of n which can be calculated from a relation easily derived from Eq. (7)

$$n = \frac{\Theta}{2T_c} \cdot \frac{\frac{1}{2}(\gamma+1) - 1}{\ln[\frac{1}{2}(\gamma+1)]} + \frac{3}{4} \tag{23}$$

Values of the index n were calculated for the first six propellant combinations listed in Table III and with the results given in Table VI.

TABLE VI

EFFECTIVE VALUES OF $d(\ln \sigma)/d(\ln T)$ FOR CESIUM SEEDING IN ROCKET MOTOR APPLICATIONS

Propellant	T_c	Θ/T_c	γ	n
Lox-NH_3	3010	14.8	1.23	8.6
Lox-Gasolene	3295	13.6	1.22	7.9
Lox-Hydrazine	2750	16.3	1.23	9.4
Lox-Kerosene	3350	13.3	1.24	7.8
F_2-Hydrazine	4430	10.1	1.33	6.2
N_2O_4-Hydrazine	2975	15.0	1.27	8.8

Thus the equilibrium electrical conductivity σ would vary as almost the 10th power of the absolute temperature for lox-hydrazine and as about the 6th power of the temperature for flourine-hydrazine. For seed materials other than cesium,

these exponents would be even larger (almost in the ratio Θ/Θ_{Cs}).

In relating this behavior to the anticipated effect of the specific heat ratio γ on the interaction parameter Q, it is then not surprising that values of γ giving the smallest temperature change for a given pressure drop are advantageous. Since Eq. (8) indicates that $T \propto p^{(\gamma-1)/\gamma}$, it can be seen that small values of the specific heat ratio γ give the largest values of the equilibrium expansion factor E. Hence, all other factors being equal, the interaction parameter Q at the exit section will be maximized by propellant combinations having small effective heat capacity ratios.

3. Effect of Expansion Pressure Ratio for a Class of Equal Thrust Motors Expanding to the Same Back Pressure

Increased chamber pressure will decrease the factors Q_{ref}, d, and E (in the Θ/T_c range of practical interest) and, as such, tend to reduce the strength of the magnetogasdynamic interaction at the exit section. This is partially offset by the fact that higher pressures give rise to larger values of the nonequilibrium enhancement $\sigma_{ex}/\sigma_{ex,eq}$, despite the fact that (according to the Thompson mechanism) the recombination parameter C_r will also increase. Again, the decrease in the equilibrium performance parameters will outweigh the nonequilibrium gain with the result that reduced chamber pressures will generally favor increased magnetic interaction for motors of the same thrust level. This conclusion is also valid in comparing motors of the same physical size (for which a chamber pressure increase implies a thrust increase).

4. Scale Effect for Motors of the Same Pressure Level

The vertical spacing of the nonequilibrium contours (lines of constant C_r) shown in Fig. 6 suggests that, even in the nonequilibrium regime, increased size will always favor increased magnetic interaction. This is a consequence of the fact that reducing the throat diameter and, hence C_r by an order of magnitude, does not cause enough of an increase in the exit value of the conductivity to outweigh the explicit d/d_t dependence appearing in Eq. (9). In the equilibrium regime, this latter dependence on physical size is indeed the only one.

Summarizing the results of each of paragraphs (1) through (4) above, it may be said that, in the range of rocket motor interest, the following characteristics

appear to be generally desirable for MHD thrust vectoring applications:

i small values of Θ/T_c (i.e., low ionization potential seed materials in "hot" chambers)

ii small values of the specific heat ratio γ

iii moderate rather than high chamber pressures

iv large physical size

5. Accuracy of Physical Model

With regard to the absolute values predicted by the use of the analysis, several comments should be made about the accuracy of the physical model. In general, most departures from the model that might occur in practice would tend to reduce the magnitude of the obtainable control force. Factors of this type include:

(a) magnetic field inhomogeneity

(b) ion slip and Hall effects[28]

(c) electron attachment[26] to form negative ions

(d) reactions of seed material with combustion products

(e) non-uniformity of profiles of mass velocity and electrical conductivity at the nozzle exit

(f) electron removal from the jet by diffusion

Apart from factors of this type, the accuracy of the predictions may be limited for particular systems for such reasons as:

(g) the expansion process cannot be well represented by any single value of the isentropic exponent γ

(h) the temperature dependence of the electron-neutral cross-section Q_σ is not negligible[5†]

(i) the pressure and temperature dependence of the recombination coefficient for the effective electron removal process are not well described by a single power law

(j) the absolute value of the recombination coefficient under chamber conditions is not well known

etc.

---

† Any power law dependence would be easily incorporated into the present analysis. For the electron interaction with water vapor[5], $Q_\sigma \sim T^{-1}$ would be more accurate than the law used in constructing Figs. 4,5,6.

Finally, it should be remembered that even if the kinetics of electron removal were accurately known, most of the nonequilibrium results presented here (Fig. 4, 5,6) are approximate. Where high accuracy is essential, exact solutions to Eq. (B-8) should be used. It is felt that the results given here (see also Appendix B) correctly parameterize the problem, correctly represent the dominant trends, and enable rapid estimates to be made. It should also be borne in mind that even the predictions of exact solutions (see Appendix B) should not be applicable for nozzle shapes having area change histories markedly different from that considered here (see Fig. 10).

VII. CONCLUDING REMARKS

Recapitulating, several universal curves have been presented in Sections I, II and III to facilitate the prediction of control forces that can be achieved by magnetohydrodynamic means in rocket motor practice. A set of equilibrium calculations also required for this purpose has been presented for 21 propellant combinations assumed to be "seeded" with small amounts of an easily ionized material. Since, in principle, the nozzle expansion process can result in electrical conductivities at the exit section considerably greater than those corresponding to local thermodynamic equilibrium, a graphical method has been introduced to enable quantitative estimates to be made of the extent of this electron recombination lag as well as the conditions under which it can (very likely) be ignored. Combining these results as illustrated in Sections V and VI, it has been possible to extract some general information as to the independent factors favoring maximum exhaust jet interaction with the applied magnetic field. Some of the major factors (other than large field strength) giving rise to favorable conditions are: (a) the presence of low ionization potential materials in "hot" chambers (low Θ/T_c), (b) small values of the effective specific heat ratio γ, (c) moderate rather than extremely large chamber pressures, and (d) large physical size. It appears from the calculations carried out thus far that control forces of the order of 0.1 to 1.0 percent of the gross thrust are attainable, by applying large magnetic fields (1 to 3 Weber/meter^2) to the exhaust jets of rocket motors in the 10,000 pound thrust class over a length comparable to the exit diameter. Upper limits to the seed concentrations are considered to be in the range of 0.1 to 1.0 percent. With the use of superconducting magnet[2] coils (perhaps capable of generating 100,000 gauss fields), side thrusts of the order of several percent of the gross thrust are predicted. Interestingly enough, nonequilibrium effects are

tentatively estimated to be quite small over a wide range of conditions likely to be encountered in rocket motor practice and, moreover, the factors favoring large nonequilibrium gains are predominantly those associated with small equilibrium values of the interaction parameter. The net effect is that control force expectations of this order of magnitude generally apply to both the equilibrium as well as nonequilibrium cases envisioned. Whether these control forces are sufficient to justify a serious effort in this direction remains to be seen, since economic and technological factors are involved which have not even been touched upon here. Insofar as the material presented here would provide perspective and input information for such a study, it is hoped that this report will prove useful.

VIII. REFERENCES

[1] Elssaser, W. M.: "Review of Magnetohydrodynamics" Am. J. Phys., 23, 590 (1955) and 24, 85 (1956); see also: Cowling, T. G.: Magnetohydrodynamics Interscience Tracts on Physics and Astronomy, No. 4, 1957 (New York); and: Steketee, J. A.: "An Introduction to the Equations of Magnetogasdynamics" University of Toronto, Institute of Aerophysics, UTIA Rev., No. 9, April 1957

[2] Anon.: News Release: "Superconducting Magnet Demonstrated by Westinghouse Engineers" Astronautics (publication of the American Rocket Society), 6, 115 (1961); see also: Physics Today (publication of the American Institute of Physics), 14, 65 (1961)

[3] Chapman, S. and Cowling, T. G.: The Mathematical Theory of Non-Uniform Gases Cambridge University Press, p. 120 (1952); see also: Sherman, A.: "Calculation of Electrical Conductivity of Ionized Gases" ARS Journal, 30, 559-560 (1960)

[4] Moffatt, W. C.: "The Thermodynamic and Electrical Properties of Dissociated Combustion Gases" Massachusetts Institute of Technology, Magnetogasdynamics Laboratory, Report No. 61-5, May 1961; see also: "The Thermodynamic and Electrical Properties of the H-C-N-O-K System" Paper No. 10, pp. 126-132, Progress in International Research on Thermodynamic and Transport Properties Academic Press, New York, 1962

[5] Gardner, J. H.: Ramo Wooldridge Report GM-00-4230-00013, September 11, 1957; see also: Molmud, P.: "Electron-Ion Three-Body Recombination in Radially Expanding Gas Flow" Space Technology Laboratories, TR-60-0000-09058, February 24, 1960

[6] Hodgman, C. D., Weast, R. C. and Selby, S. M., Eds.: Handbook of Chemistry and Physics 42nd Edition, Chemical Rubber Publishing Co., Cleveland, Ohio, pp. 2549-2551 (1960)

[7] Rosa, R. J.: "Physical Principles of Magnetohydrodynamic Power Generation" AVCO Research Report 69, January 1960

[8] Sherman, A.: "The Electrical Conductivity of Seeded Inert Gases" General Electric Company, Flight Propulsion Laboratory, Report No. R 60 FPD 237, March 17, 1960

[9] Saha, M. N. and Srivastava, B. N.: A Treatise on Heat 3rd Edition, Chapter 18, Part 16, pp. 793 ff., Indian Press, Allahabad, 1950

[10] Rosner, D. E.: "Calculation of Equilibria in Thermally Ionized Gaseous Mixtures - The Saha Equation" AeroChem TM-11, ASTIA AD 236-199, AFOSR TN 60-888, September 1958; see also: Duclos, D. P., and Cambel, A. B.: "The Equation of State of an Ionized Gas" Paper No. 55, pp. 601-617, Progress in International Research on Thermodynamic and Transport Properties, Academic Press, New York, 1962

[11] Kerrebrock, J. L.: "Electrode Boundary Layers in Direct Current Plasma Accelerators" J. Aero/Space Sciences, 28, 631-643 (1961); see also: "Nonequilibrium Effects on Conductivity and Electrode Heat Transfer in Ionized Gases" California Institute of Technology, Daniel and Florence Guggenheim Jet Propulsion Center, Technical Note No. 4, AFOSR 165, November 1960

[12] Shapiro, A. H.: The Dynamics and Thermodynamics of Compressible Fluid Flow Ronald Press, New York, 1953

[13] Sutton, G. P.: Rocket Propulsion Elements J. Wiley, New York, 2nd Edition, 1956; see also: Summerfield, M.: "The Liquid Propellant Rocket Engine" Chapter 5, Section G.6: Cooling of Rocket Motors, p. 490-510, Vol. 12 of High Speed Aero and Jet Propulsion, Jet Propulsion Engines, Princeton Univsity Press, 1959

[14] Zucrow, M. J.: Principles of Jet Propulsion and Gas Turbines John Wiley and Sons, New York, 1948

[15] Barrere, M., Jaumotte, A., Fraeijs de Veubeke, B., and Vandenkerckhove, J.: Rocket Propulsion Amsterdam: Elsevier Co., p. 219, 1960

[16] Smith, F.: "On the Analysis of Recombination Reactions in Expanding Gas Streams" Seventh Symposium on Combustion (at London), pp. 93-97, Butterworth's Scientific Publications, London, 1959

[17] Eschenroeder, A. Q. and Daiber, J. W.: "Nonequilibrium Ionization in a Shock Tunnel Flow" ARS Journal, 31, 1, 94-96 (1961); see also: Bray, K. N. C. and Wilson, J. A.: "A Preliminary Study of Ionic Recombination of Argon in Wind Tunnel Nozzles" University of Southampton, Dept. of Aeronautics and Astronautics, Report No. 134, February 1960

[18] Bell Aircraft Corporation: Pocket Data for Rocket Engines, Bell Aircraft Corporation, Buffalo, New York, 1953; see also: Callery Chemical Co.: Propellant Performance Data, Callery Chemical Co., 1961

[19] Gordon, S., and McBride, B. J.: "Theoretical Performance of Liquid Hydrogen with Liquid Oxygen as a Rocket Propellant" NASA Memorandum 5-21-59E, June 1959

[20] Rocketdyne Theoretical Chemistry Unit: "Theoretical Performance of Rocket Propellant Combinations" Rocketdyne, Division of North American Aviation, Inc., Publication 573-A-2 (1961)

[21] Bray, K. N. C.: "Departure from Dissociation Equilibrium in a Hypersonic Nozzle" Aeronautical Research Council, Report 19,983, March 1958 (England); see also: Wegener, P. P.: "Experiments on the Departure from Chemical Equilibrium in a Supersonic Flow" ARS Journal, 30, 322-329 (1960)

[22] Hall, J. G. and Russo, A. L.: "Studies of Chemical Nonequilibrium in Hypersonic Nozzle Flows" Kinetics, Equilibria and Performance of High Temperature Systems, Paper No. 30, pp. 219-231 (G. S. Bahn and E. E. Zukoski, Eds.) Butterworth's, Washington, D. C., 1960

[23] von Engel, A.: Ionized Gases Oxford, University Press, London, 1955

[24] Cobine, J. D.: Gaseous Conductors Dover Publications, New York, 1958

[25] Brown, S. C.: "Conduction of Electricity in Gases" Chapter 10, pp. 4-159 to 4-175, Handbook of Physics, E. U. Condon and H. Odishaw, Eds., McGraw-Hill Book Co., New York, 1958

[26] Calcote, H. F.: "Relaxation Processes in Plasma" Third Biennial Gas Dynamics Symposium, Northwestern University, Evanston, Illinois, August 24-26, 1959; Dynamics of Conducting Gases, Northwestern University Press, Evanston, pp. 36-50, 1960

[27] Bush, W. B.: "The Stagnation-Point Boundary Layer in the Presence of an Applied Magnetic Field" J. Aero/Space Sci., 28, 610-611, 630 (1961)

[28] Brunner, M. J.: "The Effects of Hall and Ion Slip on the Electrical Conductivity of Partially Ionized Gases for Magnetohydrodynamic Re-Entry Vehicle Application" ASME Paper No. 61-WA-176; Presented at the Winter Annual Meeting ASME, November 26, December 1, 1961, New York, New York

[29] Dimmock, T. H., Miller, G. F., Nichol, J. J. and Kineyko, W. R.: "The Electrical Properties of Ionized Flames - Part II, Electrostatic and Magnetohydrodynamic Deflection" Thiokol Chemical Corporation, Reaction Motors Division, Report AFOSR-990, August 1961

[30] Staff of Aerodynamics Group, Applied Physics Laboratory, Johns Hopkins University, Silver Spring, Md.: Handbook of Supersonic Aerodynamics, pp. 4.93-4.96, Washington, D. C., April 1, 1950

APPENDIX A

TRAJECTORY ANALYSIS: MAGNETOGASDYNAMIC JET DEFLECTION

Using an approach analogous to that adopted by Dimmock[29] etal. for finding the deflection of flame gas in the presence of crossed electrical and magnetic fields, it is possible to obtain estimates for the extent of jet deflection in the presence of a magnetic field alone. In this case, we assume that a fluid parcel of unit volume and mass ρ will be acted upon solely by the Lorenz force $\bar{j} \times \bar{B}$, where the current $\bar{j}$ is induced by the gas motion through the field in accord with $\bar{j} = \sigma(\bar{c} \times \bar{B})$. If the magnetic field is in the x-y plane, then the equations of motion for the fluid parcel shown in Fig. 1 take the form

$$\rho\ddot{x} = -\sigma(uB_y - vB_x)B_y \tag{A-1}$$

$$\rho\ddot{y} = \sigma(uB_y - vB_x)B_x \tag{A-2}$$

The initial conditions, corresponding to the undisturbed gas flow, are taken to be

$$x(0) = 0 \qquad \dot{x}(0) = c_o \tag{A-3}$$

$$y(0) = 0 \qquad \dot{y}(0) = 0 \tag{A-4}$$

Before proceeding, it is convenient to introduce the following definitions and nondimensionalization

$$\begin{aligned} X &\equiv x/d \qquad \tau \equiv c_o t/d \\ Y &\equiv y/d \qquad Q \equiv \sigma B^2 d/(\rho c_o) \end{aligned} \tag{A-5}$$

We further take the impressed magnetic field to have a magnitude B and an inclination angle θ with the x axis. Then, using primes to represent differentiation with respect to τ, the governing set of equations assumes the form

$$Q^{-1} X'' = -X' \sin^2\theta + Y' \sin\theta \cos\theta \tag{A-6}$$

$$Q^{-1} Y'' = X' \sin\theta \cos\theta - Y' \cos^2\theta \tag{A-7}$$

with the corresponding initial conditions

$$X(0) = 0 \qquad X'(0) = 1 \tag{A-8}$$

$$Y(0) = 0 \qquad Y'(0) = 0 \tag{A-9}$$

In writing Eqs. (A-6) and (A-7), it has been assumed that the induced magnetic field may be neglected. The solution to Eqs. (A-6) and (A-7), subject to conditions (A-8) and (A-9), is found to be

$$X(\tau) = Q^{-1} \sin^2\theta[1 - \exp(-Q\tau)] + \tau \cos^2\theta \tag{A-10}$$

$$X'(\tau) = 1 - \sin^2\theta[1 - \exp(-Q\tau)] \tag{A-11}$$

$$Y(\tau) = Q^{-1} \sin\theta \cos\theta\left[Q\tau - [1 - \exp(-Q\tau)]\right] \tag{A-12}$$

$$Y'(\tau) = \sin\theta \cos\theta[1 - \exp(-Q\tau)] \tag{A-13}$$

Since the jet turning angle β will be given by $\tan^{-1}[Y'(\tau)/X'(\tau)]$ and the resulting thrusts are given respectively by $F_y/F_o = Y'(\tau)$ and $F_x/F_o = X'(\tau)$, we have

$$\beta = \tan^{-1}\left[\frac{\sin\theta \cos\theta[1 - \exp(-Q\tau)]}{1 - \sin^2\theta[1 - \exp(-Q\tau)]}\right] \tag{A-14}$$

$$F_y/F_o = \sin\theta \cos\theta[1 - \exp(-Q\tau)] \tag{A-15}$$

$$F_x/F_o = 1 - \sin^2\theta[1 - \exp(-Q\tau)] \tag{A-16}$$

Finally, from Eq. (A-11) the time spent in a field of axial extent L is found to be the solution of

$$L/d = Q^{-1} \sin^2\theta[1 - \exp(-Q\tau)] + \tau \cos^2\theta \tag{A-17}$$

For small $Q\tau$ [*i.e.* small $\sigma B^2 x/(\rho c_o)$] τ and L/d become indistinguishable from one another and F_y/F_o (written hereafter as $F_\perp/F_o$) approaches

$$F_\perp/F_o \rightarrow \sin\theta \cos\theta \cdot (L/d) \cdot Q \qquad \text{(A-18)}$$

The relation between the transverse thrust $F_\perp/F_o$, interaction parameter Q, and field extent parameter L/d is shown graphically in Fig. 2 for the optimum field inclination, $\theta = 45^o$. For values of Q smaller than 10^{-2}, the asymptotic result (A-18) can be used with good accuracy, and this is usually the case in practice. Note that in this extreme the transverse thrust will increase <u>linearly</u> with Q, and that if $\theta = 45^o$ and L/d = 1, then $F_\perp/F_o \rightarrow \frac{1}{2} Q$. The asymptotic extreme $Q \rightarrow \infty$ is of more theoretical interest. In this extreme $F_\perp/F_o \rightarrow \frac{1}{2}$, corresponding to a maximum jet deflection equal to the 45^o field inclination.

APPENDIX B

ELECTRON-ION RECOMBINATION LAGS

Formulation

To predict the extent of departures from equilibrium in nozzle flows, one must examine the conservation equation governing changes in the ion or electron concentration. Since we are really interested in the electrical conductivity of the gas and its variation through the nozzle, it is convenient to transform this equation into one in which the conductivity σ is the dependent variable, in accord with Eq. (2). The particular case to be considered here is one in which a seed material, present in dilute amounts, contributes most of the electrons to the gas via the reaction

$$S \rightarrow S^+ + e \tag{B-1}$$

In the course of the expansion, the reverse reaction begins to dominate (B-1)

$$S^+ + e \rightarrow S \tag{B-2}$$

and if the expansion is rapid enough, S^+, e, and S may not be in equilibrium with one another downstream of the combustion chamber. Regardless of the actual molecularity, the kinetics of reaction (B-2) are conventionally described by a phenomenological law of the form

$$\frac{dn_e}{dt} = - \alpha_r n_e n_+ \tag{B-3}$$

where α_r is referred to as the recombination coefficient. With the condition of electrical neutrality ($n_e = n_+$), Eq. (B-3) becomes

$$\frac{dn_e}{dt} = - \alpha_r (n_e)^2 \tag{B-4}$$

It follows that at any point in the nozzle the <u>net</u> rate of electron production can be expressed as $- \alpha_r [(n_e)^2 - (n_{e,eq})^2]$ in units of number of electrons per unit time and volume. Therefore, the <u>mass</u> source term $\dot{w}_e$ appearing in

the conservation equation for electrons is of the form

$$\dot{w}_e = - \alpha_r m_e[(n_e)^2 - (n_{e,eq})^2] \tag{B-5}$$

where m_e is the mass of the electron. In terms of the mass fraction, $m_e n_e/\rho$, of electrons, the steady flow conservation equation therefore becomes

$$\rho u \frac{d}{dx}\left(\frac{m_e n_e}{\rho}\right) = - \alpha_r m_e[(n_e)^2 - (n_{e,eq})^2] \tag{B-6}$$

As already suggested, it is convenient to nondimensionalize and transform Eq. (B-6) into one governing changes in the electrical conductivity σ itself. To do this, we introduce the following definitions

$$\begin{aligned} \bar{p} &\equiv p/p_c & \bar{u} &\equiv u/c^* \\ \bar{T} &\equiv T/T_c & \bar{x} &\equiv x/D_t \\ \bar{\sigma} &\equiv \sigma/\sigma_c & \bar{\sigma}_{eq} &= \sigma_{eq}/\sigma_{c,eq} \\ \bar{\alpha}_r &\equiv \alpha_r/\alpha_{r,c} = \bar{p}^{\omega_p} \bar{T}^{\omega_T} \end{aligned} \tag{B-7}$$

and denote the group $\alpha_{r,c}\, n_{e,c}\, D_t/c^*$, which naturally makes its appearance, as the <u>recombination parameter</u>, C_r. We note that C_r is nothing more than the ratio of the characteristic flow time $\tau_{flow} = D_t/c^*$ to the electron half life $\tau_{chem} = (\alpha_{r,c}\, n_{e,c})^{-1}$ in the chamber. The resulting equation for the nonequilibrium conductivity distribution $\bar{\sigma}(\bar{x})$ becomes

$$\frac{d\bar{\sigma}}{d\bar{x}} = - C_r(\bar{p})^{\omega_p+1} (\bar{T})^{\omega_T-\frac{1}{2}} (\bar{u})^{-1}[(\bar{\sigma})^2 - (\bar{\sigma}_{eq})^2] - \tfrac{1}{2} \frac{\bar{\sigma}}{\bar{T}} \frac{d\bar{T}}{d\bar{x}} \tag{B-8}$$

This equation is in a convenient form since the variation of $\bar{\sigma}_{eq}$ through a nozzle[5] has already been calculated and discussed (see Section III). Moreover, the relations between $\bar{u}$, $\bar{p}$, and T are particularly simple for isentropic nozzle flow, <u>i.e.</u>

$$\bar{p} = (\bar{T})^{\frac{\gamma}{\gamma-1}} \tag{B-9}$$

and

$$\bar{u} = [2\gamma/(\gamma - 1)]^{\frac{1}{2}} \Omega\, (1 - \bar{T})^{\frac{1}{2}} \tag{B-10}$$

where $$\Omega(\gamma) \equiv (\gamma)^{\frac{1}{2}}[2/(\gamma+1)]^{\frac{\gamma+1}{2(\gamma-1)}} \qquad \text{(B-11)}$$

is a well tabulated function[14] of the specific heat ratio γ. Exact solutions to Eq. (B-8) could therefore be obtained by numerical integration for any class of nozzle shapes. However, before embarking on such a program, it was decided to extract some approximate results without performing any integrations. Indeed, the results described below (which are reported in the text) were obtained using approximations of the type which have been successfully introduced by Bray and Hall *etal*. for chemically reacting nozzle flows. A comparison of these results with a more exact treatment will also be included.

"Sudden Freeze" Approximation

The principle underlying these methods is that the transition region between equilibrium and frozen flow is frequently small enough to disregard. The actual distribution of species in the nozzle is therefore often well represented by patching the equilibrium and frozen solutions together at a suitable "freeze point". Methods of determining this freeze point differ somewhat; however, for the present purposes, any of the methods commonly used should suffice. What is important is that this point, and the corresponding electron mole fraction, can be obtained from the properties of the equilibrium curve itself.

A method of determining the freeze point paralleling that of Ref. 17 would proceed as follows. At the freeze point it is approximately true that

$$-\frac{d\bar{\sigma}}{d\bar{x}} \sim C_r(\bar{p})^{\omega_p+1}(\bar{T})^{\omega_T-\frac{1}{2}}(\bar{\sigma}_{eq})^2 + \tfrac{1}{2}\frac{\bar{\sigma}_{eq}}{\bar{T}}\frac{d\bar{T}}{d\bar{x}} \qquad \text{(B-12)}$$

If, in that region, we introduce the "average" slope

$$-\frac{d\bar{\sigma}}{d\bar{x}} \simeq -\tfrac{1}{2}\left[\left(\frac{d\bar{\sigma}}{d\bar{x}}\right)_{eq} + \left(\frac{d\bar{\sigma}}{d\bar{x}}\right)_{f}\right] \qquad \text{(B-13)}$$

Then freezing should occur where the following equality is achieved

$$\tfrac{1}{2}\bar{u}(\bar{p})^{-(\omega_p+1)}(\bar{T})^{-(\omega_T-\frac{1}{2})}(\bar{\sigma}_{eq})^{-2}\left[\left|-\frac{d\bar{\sigma}_{eq}}{d\bar{x}}\right| + \tfrac{1}{2}\frac{\bar{\sigma}_{eq}}{\bar{T}}\left|-\frac{d\bar{T}}{d\bar{x}}\right|\right] \tilde{=} C_r \qquad \text{(B-14)}$$

For a nozzle of any prescribed shape, the quantity on the left hand side of this equation can be tabulated as a function of Mach number or $\bar{p}$. Thus the value of $\bar{p}$, and hence the corresponding conductivity $\bar{\sigma}_f$, can be obtained for any desired value of the rate parameter C_r.

Calculation Procedure

To carry this procedure through in a realistic case, calculations were performed for the nozzle shape shown in Fig. 7. This axisymmetric nozzle includes a conical expansion section with a half angle Φ of 15°. The cone is in turn tangent to the inside of a torus which comprises the entire converging section (and a small portion of the expansion section). The torus is sized such that the radius of curvature at the throat of the resulting nozzle is equal to its throat diameter D_t. It is then a simple matter to express the area and its spatial rate of change within this nozzle. For $\bar{x} \ll 1 - \cos(\frac{\pi}{2} + \Phi)$, the dimensionless area distribution is found to be

$$\bar{A} \equiv A/A_t = [1 + 2\,(1 - \sin\vartheta)]^2 \qquad \text{(B-15)}$$

where ϑ and $\bar{x}$ are related in accord with $\bar{x} = 1 - \cos\vartheta$. Therefore, in this range

$$\frac{d\bar{A}}{d\bar{x}} = -\frac{4}{\tan\vartheta}\cdot(\bar{A})^{\frac{1}{2}} \qquad \text{(B-16)}$$

On the other hand, in the conical section

$$\frac{d\bar{A}}{d\bar{x}} = 4\tan\Phi\,(\bar{A})^{\frac{1}{2}} \qquad \text{(B-17)}$$

The derivatives required to proceed are $d\bar{\sigma}_{eq}/d\bar{x}$ and $d\bar{T}/d\bar{x}$. It is convenient to calculate these quantities by decomposing them in accord with the chain rule as follows

$$\frac{d\bar{\sigma}_{eq}}{d\bar{x}} = \left[\left(\frac{\partial\bar{\sigma}_{eq}}{\partial\bar{T}}\right)_{\bar{p}} \frac{d\bar{T}}{dM} + \left(\frac{\partial\bar{\sigma}_{eq}}{\partial\bar{p}}\right)_{\bar{T}} \frac{d\bar{p}}{dM}\right]\left(\frac{d\bar{A}}{dM}\right)^{-1}\left(\frac{d\bar{A}}{d\bar{x}}\right) \tag{B-18}$$

$$\frac{d\bar{T}}{d\bar{x}} = \left(\frac{d\bar{T}}{dM}\right)\left(\frac{d\bar{A}}{dM}\right)^{-1} \frac{d\bar{A}}{d\bar{x}} \tag{B-19}$$

An expression for each individual derivative is now available. In particular, it can be verified from Eq. (7) that

$$\left(\frac{\partial\bar{\sigma}_{eq}}{\partial\bar{T}}\right)_{\bar{p}} = \bar{\sigma}_{eq}\left[\frac{\Theta}{2T_c}\left(\frac{1}{\bar{T}}\right)^2 + \frac{3}{4}\left(\frac{1}{\bar{T}}\right)^{\frac{1}{2}}\right] \tag{B-20}$$

$$\left(\frac{\partial\bar{\sigma}_{eq}}{\partial\bar{p}}\right)_{\bar{T}} = -\frac{1}{2\bar{p}} \cdot \bar{\sigma}_{eq} \tag{B-21}$$

From the isentropic flow relations, one can obtain the following three derivatives with respect to Mach number

$$\frac{d\bar{T}}{dM} = -(\gamma - 1)(\bar{T})^2 M \tag{B-22}$$

$$\frac{d\bar{p}}{dM} = -\gamma \bar{p} \bar{T} M \tag{B-23}$$

$$\frac{d\bar{A}}{dM} = (M^2 - 1)\bar{T}\left(\frac{\bar{A}}{M}\right) \tag{B-24}$$

Using the relations given above and a set of isentropic flow tables[30], it is then possible to make a plot of the left hand side of Eq. (B-14) as a function of the Mach number for any choice of the coefficients ω_T and ω_p (i.e., for any recombination mechanism). Having done this (see Fig. 12), the conductivity $\bar{\sigma}_f$ corresponding to any prescribed value of the rate parameter C_r can be read off a figure such as Fig. 6. If the carrier gas expansion proceeds past this point, then $\bar{\sigma}$ will thereafter vary in accord with Eq. (17) given in the text. Because pressure and temperature bear a power law relationship with one another, a

convenient way of presenting these results is to superpose contours of constant recombination parameter C_r on a log-log plot of equilibrium conductivity versus expansion pressure ratio (c.f. Figs. 4,5,6). If the contour corresponding to the best estimate of C_r (for a particular problem) crosses the equilibrium curve before the exit pressure is reached, then the approximate variation of conductivity through the nozzle is obtained by simply combining the equilibrium variation upstream of the freeze point with a straight line (on the $\log\bar{\sigma}$ - $\log \frac{1}{p}$ plane) corresponding to the frozen portion of the flow. If the electron-neutral collision cross-section Q_σ is temperature insensitive, the slope of these lines (representing lines of constant electron mole fraction) is $\frac{1}{2}[(\gamma - 1)/\gamma]$. For the case of $\gamma = 1.2$, the slope is that of the hypotenuse of the triangle depicted in Figs. 4, 5 and 6. This general procedure is described in Section III of the text.

Selection of Realistic Parameters

A discussion of the choice of the exponents ω_p and ω_T is in order since the conclusions depend quite markedly on the choice ultimately made. It is recalled that these parameters describe the dependence of the recombination coefficient α_r on pressure and temperature and, as such, reflect differences in the microscopic mechanism of ion recombination. Several self-consistent sets are included in Table VI, together with remarks on the applicability of each.

For a fixed temperature level these mechanisms are such that each may become dominant at an appropriate pressure level. This accounts in part for the shape of such recombination coefficient curves as shown in Fig. 11. The presence of pressure independent mechanisms (such as the last two given in Table VII) would have the effect of introducing pressure independent lower bounds on α_r not shown in Fig. 11. It should also be remarked that the pressure regimes at which these "exchanges" of mechanism occur themselves shift considerably with changes in the temperature level. This fact appears to be extremely important in rocket motor applications since statements, such as "the Thompson mechanism should not apply at pressures over one atmosphere", often leave unstated the temperature level at which this conclusion is justified. At rocket motor temperatures the Thompson mechanism may actually be applicable to 100 atmospheres, but this is an unanswered question for experiment to decide. It is also true that while the pressure range of interest in rocket motor applications may appear to pass through one of the transition regions on an isothermal plot of α_r vs pressure, this may not be the

case in the actual expansion because of the corresponding temperature changes (c.f. trajectory shown on Fig. 11 for $\gamma = 1.2$) in isentropic nozzle flow.

TABLE VII

PRESSURE AND TEMPERATURE DEPENDENCE OF THE ION RECOMBINATION COEFFICIENT[23,24,25]

Mechanism	Theory	ω_p	ω_T	Remarks
Three-Body	J.J., G.P. Thompson (1924)	$+1 \rightarrow 0$	$-\frac{7}{2} \rightarrow -\frac{5}{2}$	Thermal velocity determines rate of successful encounters
Three Body-Mobility Controlled	P. Langevin (1903)	-1	$+\frac{1}{2}$	Thermal velocity neglected compared with that due to field induced drift. May not apply to electron-ion recombination
Two-Body; Dissociative	D.R. Bates (1950)	0	$-\frac{3}{2} \rightarrow -\frac{1}{2}$	May apply to monatomic gases due to ion clustering
Radiative	Strueckelberg and Morse (1930) etal.	0	-	$\alpha_r < 10^{-12}$ for ion-electron recombination at ambient temperature
'Spontaneous' (dielectronic)		0	-	$\alpha_r \sim 10^{-9}$ to 10^{-12} at ambient temperature for ion-electron recombination

As described in the text, calculations have been carried out for both the Thompson and Langevin mechanisms and it is found that for comparable values of the recombination parameter C_r, the Thompson mechanism predicts much larger deviations from equilibrium (i.e., earlier freeze). This is not surprising, particularly in view of the important difference in pressure dependence (see Table VII). Interestingly enough, the Langevin values of ω_p and ω_T are just those required to annihilate the explicit pressure and temperature dependence of the first term on the right hand side of Eq. (B-8); i.e., for this case

$$\frac{d\bar{\sigma}}{d\bar{x}} = - C_r \bar{u}^{-1} [\bar{\sigma}^2 - \bar{\sigma}_{eq}^2] - \tfrac{1}{2} \bar{\sigma} \bar{T}^{-1} \frac{d\bar{T}}{d\bar{x}} \qquad \text{(B-25)}$$

However, this is more of a curiousity than an essential simplification.

Accuracy of the Sudden Freeze Approximation; Improved Approximations

While the "sudden freeze" technique lends itself to the presentation of the effects of ionization nonequilibrium in a compact form suitable for rapid graphical calculation (see Figs. 4,5,6), where accuracy is important, improved solutions will probably be necessary. For, in reality, the transition from near equilibrium to highly nonequilibrium flow will take place over a range of a Mach number and strict constancy of the electron mole fraction will never be achieved. It is then of interest to investigate the nature of the exact solutions to Eq. (B-8), both to determine the absolute error in a "sudden freeze" approximation as well as to develop more accurate approximate procedures.

The nature of the exact solution is readily appreciated by reference to the behavior of the integral curves of Eq. (B-8), sketched in Fig. 13. One notices that over a wide Mach number range only small departures from equilibrium are "permitted" but, ultimately, the integral curves turn away from the equilibrium line. Having accomplished this, they assume an analytic form readily obtained from Eq. (B-8) by setting $\sigma^2 \gg \sigma_{eq}^2$, i.e.

$$\frac{d\bar{\sigma}}{d\bar{x}} = - C_r (\bar{p})^{\omega_p + 1} (\bar{T})^{\omega_T - \frac{1}{2}} (\bar{u})^{-1} (\bar{\sigma})^2 - \tfrac{1}{2} \frac{\bar{\sigma}}{\bar{T}} \frac{d\bar{T}}{d\bar{x}} \qquad \text{(B-26)}$$

But this equation can be integrated to obtain

$$\frac{1}{\bar{\sigma}\sqrt{\bar{T}}} - \frac{1}{\bar{\sigma}_o \sqrt{\bar{T}_o}} = C_r \int_{\bar{x}_o}^{\bar{x}} \frac{\bar{p}^{\omega_p + 1} \bar{T}^{\omega_T - 1}}{\bar{u}} \, d\bar{x} \qquad \text{(B-27)}$$

where the subscript o is used to denote any point in the nozzle. Since Mach number is a more convenient independent variable, it is useful to introduce the

function[†]

$$H(M) \equiv \int_1^M \frac{\bar{p}^{\omega_p+1}\,\bar{T}^{\omega_T-1}}{\bar{u}} \left(\frac{d\bar{A}}{d\bar{x}}\right)^{-1}\left(\frac{d\bar{A}}{dM}\right)dM \tag{B-28}$$

in terms of which Eq. (B-27) may be written (for $M > 1$)

$$\frac{1}{\bar{\sigma}\sqrt{\bar{T}}} - \frac{1}{\bar{\sigma}_o\sqrt{T_o}} = C_r[H(M) - H(M_o)] \tag{B-29}$$

These integral curves of Eq. (B-26), which make no reference to $\bar{\sigma}_{eq}$ (and, hence, are independent of Θ/T_c), are sketched in Fig. 14. A study of this figure, together with the relation between Eqs. (B-8) and (B-26), now suggests an alternate approximation method expected to be more accurate than the "sudden freeze" technique described earlier. This improved approximation method, which may be called a "maximum lower bound" technique, also patches two solutions together at an appropriate match point and is described below.[‡]

The relation between the slope fields of Eqs. (B-8) and (B-26) is such that the result of following the equilibrium curve to some point and then proceeding along an integral curve of Eq. (B-26) will always fall <u>beneath</u> an exact solution of Eq. (B-8). Clearly then the <u>maximum lower bound</u> will everywhere be obtained by following the equilibrium curve until it becomes <u>tangent</u> to an integral curve of Eq. (B-26) and then following this latter integral curve beyond the tangency point. At this tangency or "match" point (subscript m) both $\bar{\sigma}$ and $d\bar{\sigma}/dM$ are continuous, so that

$$\bar{u}(\bar{p})^{-(\omega_p+1)}\,(\bar{T})^{-(\omega_T-\frac{1}{2})}\,(\bar{\sigma}_{eq})^{-2}\left[\left(-\frac{d\bar{\sigma}_{eq}}{d\bar{x}}\right) - \tfrac{1}{2}\frac{\bar{\sigma}_{eq}}{\bar{T}}\left(\frac{d\bar{T}}{d\bar{x}}\right)\right] = C_r \tag{B-30}$$

Note that this is identical with Eq. (B-14) (the previous "freeze criterion" with the factor $\frac{1}{2}$ removed. Physically, it can be shown that m represents the point on the equilibrium curve at which the equilibrium rate of change of electron mole

---

[†] Actually H should be written $H(M;\ \gamma,\ \omega_T,\ \omega_p)$.

[‡] This improved method is equivalent to that suggested by Smith in Ref. 16.

fraction is equal to that produced by the recombination reaction alone. Fig. 15 compares the solution obtained in this way with both the exact solution and a "sudden freeze" solution. While the latter predicts the exit conductivities to within better than a factor of two, it is much less successful than the maximum lower bound method. Since, in practice, the maximum lower bound method is not much more difficult to apply, H is to be recommended for future nonequilibrium flow studies of this type. Rapid calculation using this method will be facilitated by the combined use of Fig. 16 and Table VIII. Fig. 16 shows the position of the match points m as determined from Eq. (B-30) for two distinct recombination mechanisms. Numerical values of H(M) are given in Table VIII, to be used in conjunction with Eq. (B-29).

TABLE VIII

THE FUNCTION H(M) FOR γ = 1.2 ISENTROPIC EXPANSIONS IN A $\Phi = 15^{\circ}$ HALF ANGLE CONE

M	$\bar{T}^{\frac{1}{2}}$	$\bar{p}$	H(M)†	
			3-Body‡	Dissoc.††
1.0	0.9535	0.5645	0.0000	0.0000
1.2	0.9349	0.4461	0.0169	0.0273
1.4	0.9144	0.3417	0.0482	0.0861
1.6	0.8923	0.2547	0.0796	0.1568
1.8	0.8691	0.1856	0.1063	0.2305
2.0	0.8452	0.1328	0.1274	0.3025
2.2	0.8209	0.09363	0.1433	0.3707
2.4	0.7966	0.06526	0.1549	0.4343
2.6	0.7724	0.04512	0.1634	0.4928
2.8	0.7487	0.03102	0.1694	0.5464
3.0	0.7255	0.02126	0.1736	0.5951
3.2	0.7029	0.01455	0.1767	0.6395
3.4	0.6810	$0.0_2 9957$‡‡	0.1788	0.6797
3.6	0.6600	$0.0_2 6826$	0.1803	0.7162
3.8	0.6397	$0.0_2 4692$	0.1813	0.7494
4.0	0.6202	$0.0_2 3237$	0.1821	0.7795
4.2	0.6015	$0.0_2 2243$	0.1826	0.8069
4.4	0.5836	$0.0_2 1561$	0.1830	0.8318
4.6	0.5665	$0.0_2 1092$	0.1833	0.8545
4.8	0.5501	$0.0_3 7687$	0.1835	0.8752
5.0	0.5345	$0.0_3 5440$	0.1836	0.8942

† absolute values subject to ± 2 digit maximum error in last place tabulated

‡ Thompson mechanism; $\omega_p = +1$, $\omega_I = -7/2$

†† Dissociative mechanism; $\omega_p = 0$, $\omega_I = -3/2$

‡‡ The subscript appearing on the zero to the right of the decimal point indicates the number of zeros appearing before the first non-zero digit, i.e. $0.0_2 9957 \equiv 0.009957$.

APPENDIX C

DECAY OF ELECTRICAL CONDUCTIVITY DOWNSTREAM OF THE NOZZLE

In the region beyond the nozzle the rate of change of stream tube area becomes negligible, so that all gasdynamic properties of the working fluid tend to remain constant.† However, if a departure from ionization equilibrium has occurred within the nozzle, the electron recombination reaction (B-2) persists and it is of interest to find the spatial rate of approach to ionization equilibrium for the seed material. If the distance required to return to equilibrium is much larger than the contemplated streamwise extent, L, of the magnetic field (see Fig. 1) then no significant decay of the electrical conductivity, σ, would occur within the magnetic interaction region.

In a downstream region of constant stream tube area, Eq. (B-8) simplifies considerably since

$$\begin{aligned} \bar{p} &\tilde{=} \text{constant} = \bar{p}_{ex} \\ \bar{T} &\tilde{=} \text{constant} = \bar{T}_{ex} \\ \bar{\sigma}_{eq} &\tilde{=} \text{constant} = \bar{\sigma}_{eq,ex} \\ \bar{u} &\tilde{=} \text{constant} = \bar{u}_{ex} \end{aligned} \tag{C-1}$$

As a result, the normalized electrical conductivity σ/σ_c will decay in accord with the equation

$$\frac{d\bar{\sigma}}{d\bar{x}} = - C_r \, (\bar{p}_{ex})^{\omega_p + 1} \, (\bar{T}_{ex})^{\omega_T - \frac{1}{2}} \, (\bar{u}_{ex})^{-1} \left[(\bar{\sigma})^2 - (\bar{\sigma}_{eq,ex})^2 \right] \tag{C-2}$$

In this region it is therefore convenient to introduce two new variables, the first of these being the nonequilibrium enhancement ratio, Σ, defined by

$$\Sigma \equiv \bar{\sigma}/\bar{\sigma}_{ex,eq} \tag{C-3}$$

For a specified initial value, Σ will depend only on the stretched streamwise coordinate

---

† apart from effects such as radial diffusion and turbulent mixing at the jet boundary

$$z \equiv C_r \cdot (\bar{p}_{ex})^{\omega_p+1} (\bar{T}_{ex})^{\omega_T-\frac{1}{2}} (\bar{u}_{ex})^{-1} \sigma_{ex,eq} (d_t/d_{ex}) (x/d_{ex}) \qquad (C\text{-}4)$$

Eq. (C-2) reveals that $\Sigma(z)$ must satisfy the separable first order equation

$$\Sigma' = -(\Sigma^2 - 1) \qquad (C\text{-}5)$$

subject to the initial condition $\Sigma(0) \equiv \Sigma_o$. The corresponding solution is found to be

$$\Sigma(z) = \frac{(\Sigma_o + 1) + (\Sigma_o - 1) \exp(-2z)}{(\Sigma_o + 1) - (\Sigma_o - 1) \exp(-2z)} \qquad (C\text{-}6)$$

Thus the decay of nonequilibrium electrical conductivity downstream of the nozzle is readily calculable in terms of the previous nozzle flow parameters. Results are shown in Fig. 17. Perhaps of greater interest in the present study is the <u>average</u> value $\langle\Sigma\rangle$ of the enhancement ratio Σ on the interval from 0 to z, since this average would be more representative of the overall interaction region than either the final or initial values. Fortunately, a simple expression for the average value Σ is obtainable from Eq. (C-6), <u>viz</u>.

$$\langle\Sigma\rangle = 1 + \frac{1}{z} \ln \tfrac{1}{2}[(\Sigma_o + 1) - (\Sigma_o - 1) \exp(-2z)] \qquad (C\text{-}7)$$

This relation is shown graphically in Fig. 18 and can be used to assess the importance of electron recombination downstream of the nozzle in decreasing the (spatial) average value of the nonequilibrium electrical conductivity. To facilitate combining these results with those of the nozzle expansion, analysis of Appendix B plots of the following universal function (c.f. Fig. 19) are useful

$$G(p_c/p \; ; \Theta/T_c, \gamma, \omega_T, \omega_p) \equiv \bar{p}^{\omega_p+1} \bar{T}^{\omega_T-\frac{1}{2}} \bar{u}^{-1} \bar{A}^{-\frac{1}{2}} \bar{\sigma}_{eq} \qquad (C\text{-}8)$$

With the help of this function, the downstream distance (measured in exit diameters) is readily related to the stretched coordinate z as follows

$$z = C_r \cdot G \cdot (x/d_{ex}) \qquad (C\text{-}9)$$

Here, the recombination parameter C_r has already been introduced and evaluated for the nozzle flow analysis.

To illustrate the use of these graphs, consider the case of a $\gamma = 1.2$ isentropic expansion through a pressure ratio $p_c/p = 68$. If the equilibrium ionization parameter Θ/T_c is 15 and the recombination parameter C_r has been estimated to be 10^3 we ask:

(a) What electrical conductivity is likely to prevail 10 exit diameters downstream of the nozzle exit section?

(b) What is the corresponding average value of the electrical conductivity over the first 10 exit diameters?

For simplicity we will make use of the "sudden freeze" analysis, assuming that the Thompson three-body recombination mechanism prevails. Then Fig. 6 is appropriate and we find that $\bar{\sigma}_{ex} = 0.039$ and $\bar{\sigma}_{ex,eq} = .0_223$; consequently $\Sigma_o \equiv \bar{\sigma}_{ex}/\bar{\sigma}_{ex,eq} = 17$. Fig. 19 reveals that $z = 0.0_517\ C_r \cdot (x/d_{ex})$, so that 10 diameters downstream $(x/d_{ex} = 10)$ we have $z = (0.0_517)(10^3)(10) = 1.7 \times 10^{-2}$. The value of $\Sigma(z)/\Sigma_o$ corresponding to $z = 1.7 \times 10^{-2}$ and $\Sigma_o = 17$ is found, from Fig. 17, to be about 0.78. The average value $\langle\Sigma\rangle/\Sigma_o$ is estimated from Fig. 18 to be 0.88. Therefore, the corresponding values of Σ and $\langle\Sigma\rangle$ are, respectively, $(0.78)(17) = 13$ and $0.88(17) = 15$. From the definitions of Σ and $\langle\Sigma\rangle$ and the fact that $\bar{\sigma}_{ex,eq} = 0.0_223$, we then conclude that $\bar{\sigma} = \bar{\sigma}_{ex,eq}\,\Sigma = 0.0_223(13) = .031$ and $\langle\sigma\rangle = \bar{\sigma}_{ex,eq}\langle\Sigma\rangle = (0.0_223)(15) = .034$. Thus, the electrical conductivity 10 diameters downstream of the nozzle exit section is likely to be about 3.1 percent of the electrical conductivity in the chamber. The average conductivity over the first 10 diameter length is approximately 3.4 percent of the chamber conductivity. By way of comparison, if equilibrium had been maintained everywhere, the electrical conductivity at the 10 diameter location would have been only 0.23 percent of the electrical conductivity in the chamber. As illustrated by this example, one cannot expect good precision in the use of Figs. 17 and 18. Where this is important, the complexity of Eqs. (C-6) and (C-7) is far from prohibitive and their direct use is recommended. In general, the curves presented will then be useful in revealing what regimes of operation will be encountered, and whether more precise calculations are necessary.

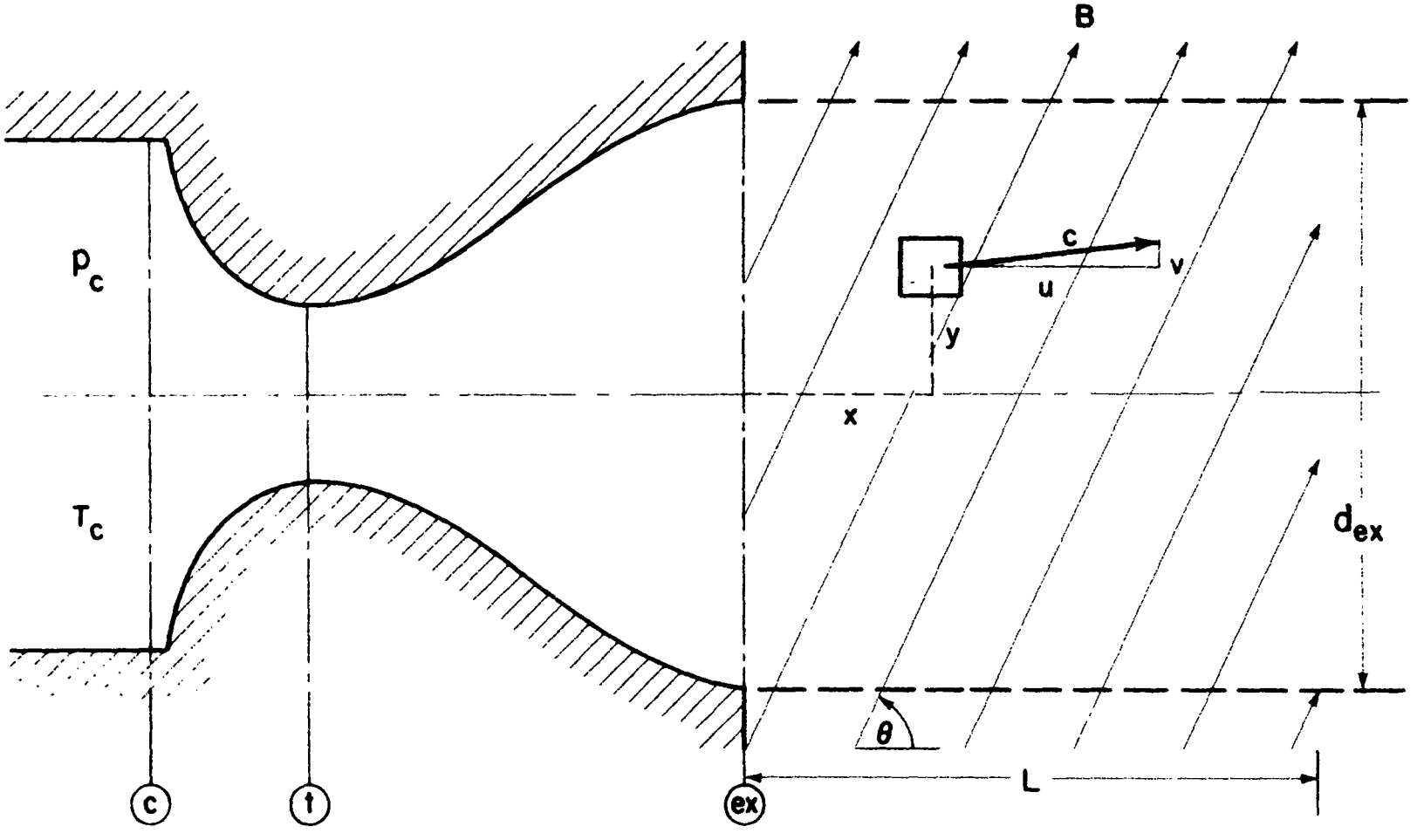

FIG. 1 GEOMETRIC CONFIGURATION: IONIZED JET PASSING THROUGH AN IMPOSED MAGNETIC FIELD

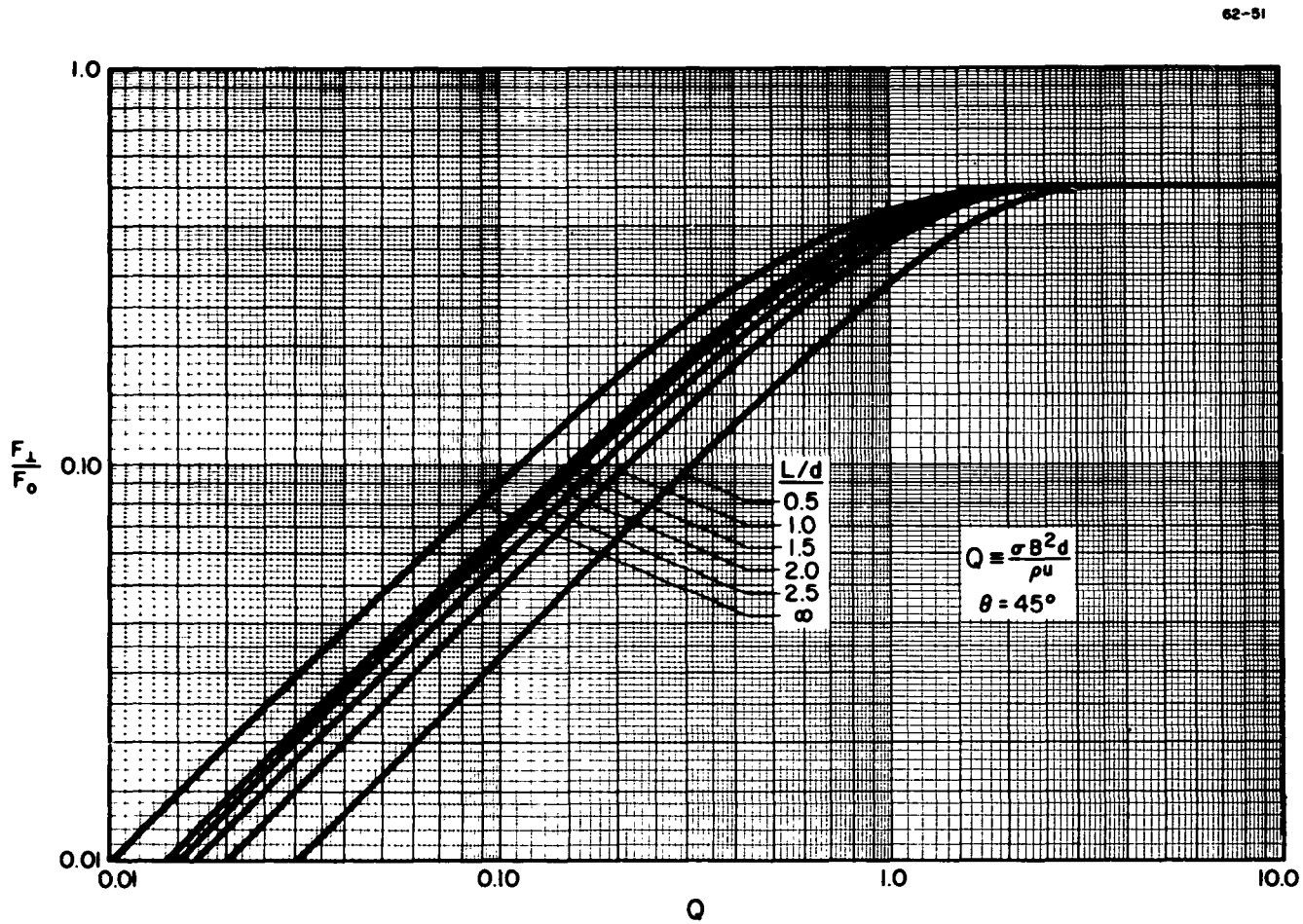

FIG. 2 DEPENDENCE OF ATTAINABLE TRANSVERSE THRUST ON THE MAGNITUDE OF THE MAGNETOGASDYNAMIC INTERACTION PARAMETER Q

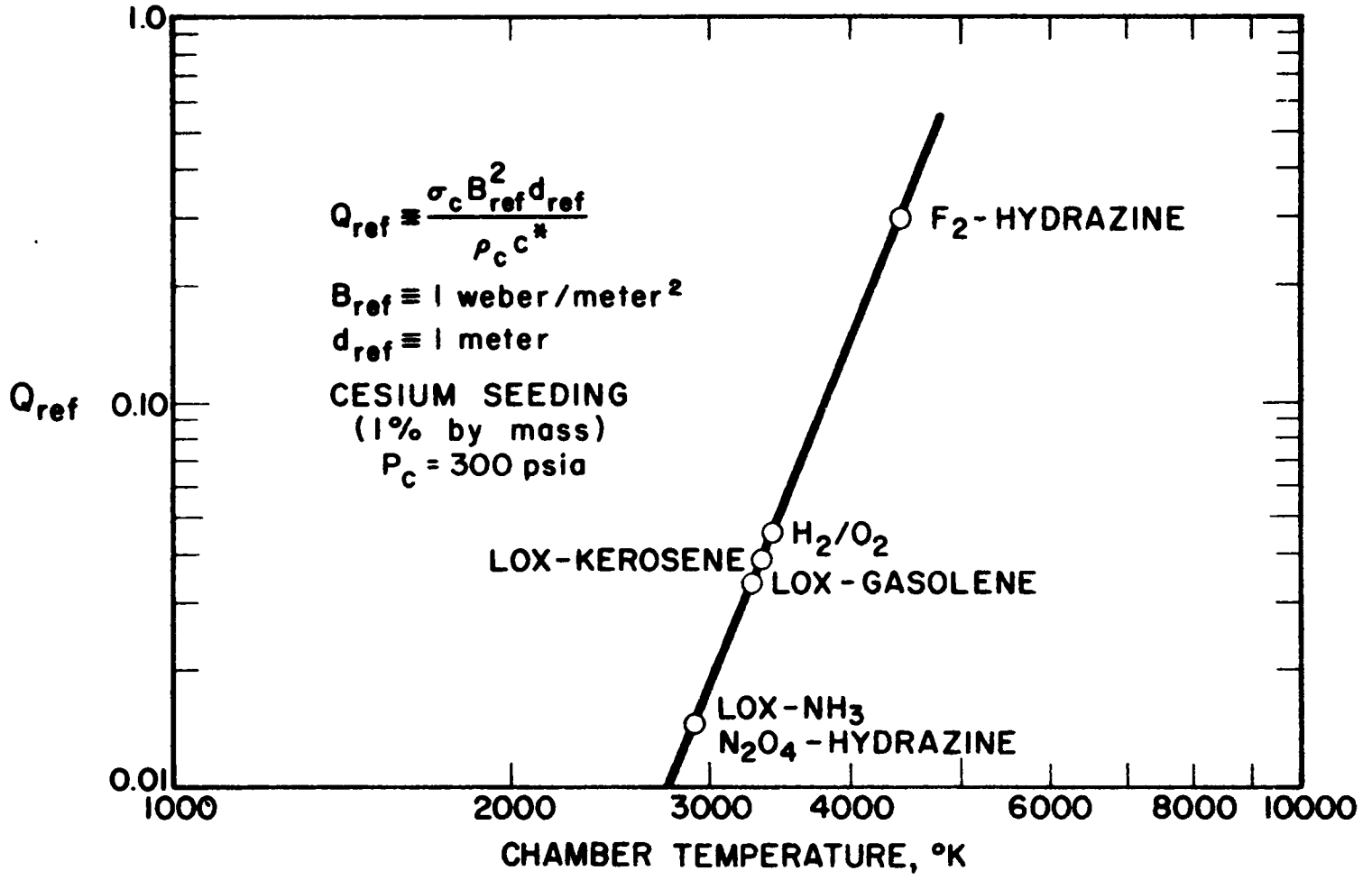

FIG. 3 CORRELATION OF Q_{ref} WITH CHAMBER TEMPERATURE FOR 300 PSIA MOTORS

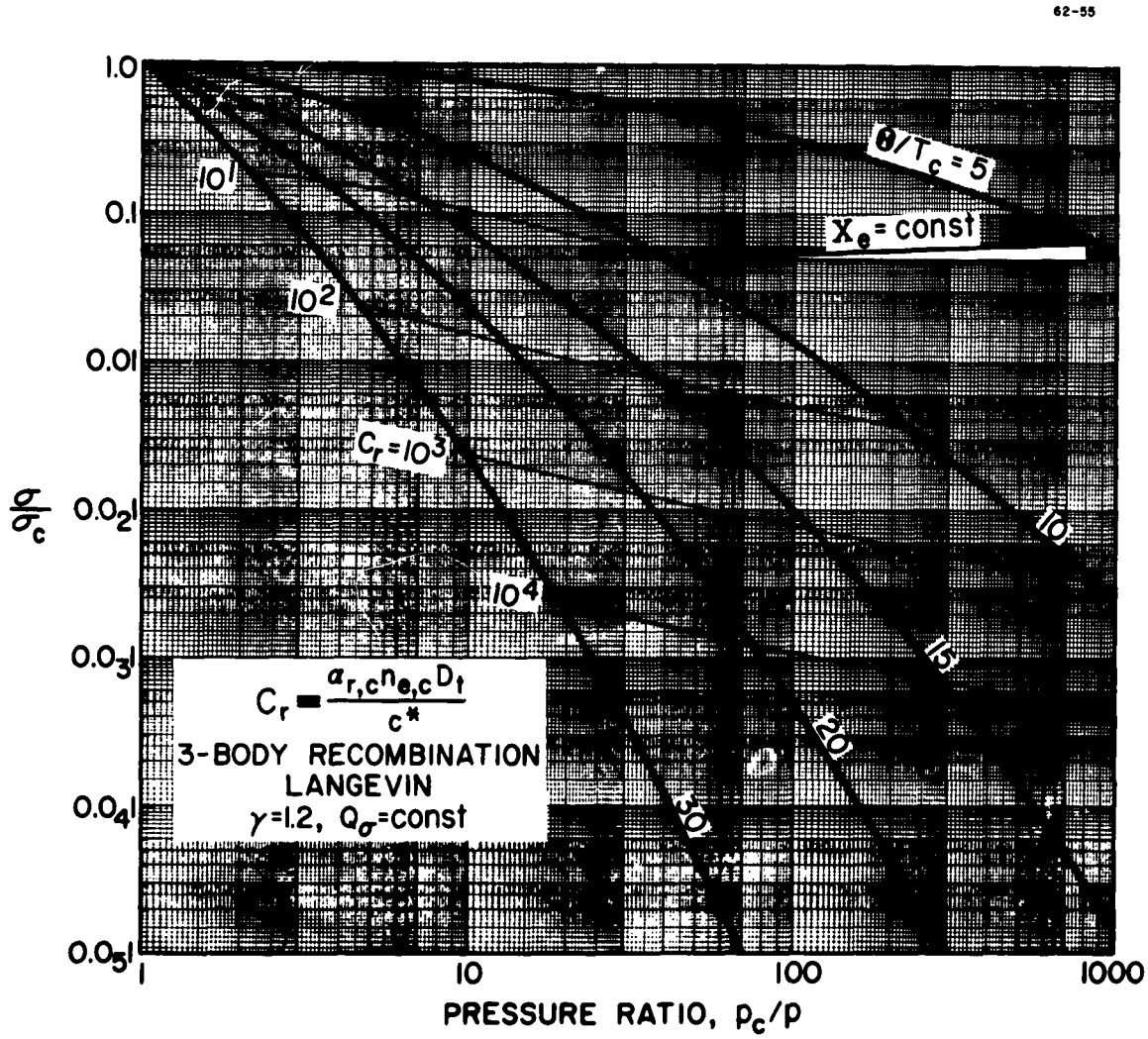

FIG. 4 THE EFFECT OF ELECTRON-ION RECOMBINATION LAG ON EXIT VALUES OF THE ELECTRICAL CONDUCTIVITY FOR ISENTROPIC NOZZLE EXPANSIONS
(γ = 1.2; Langevin Recombination)

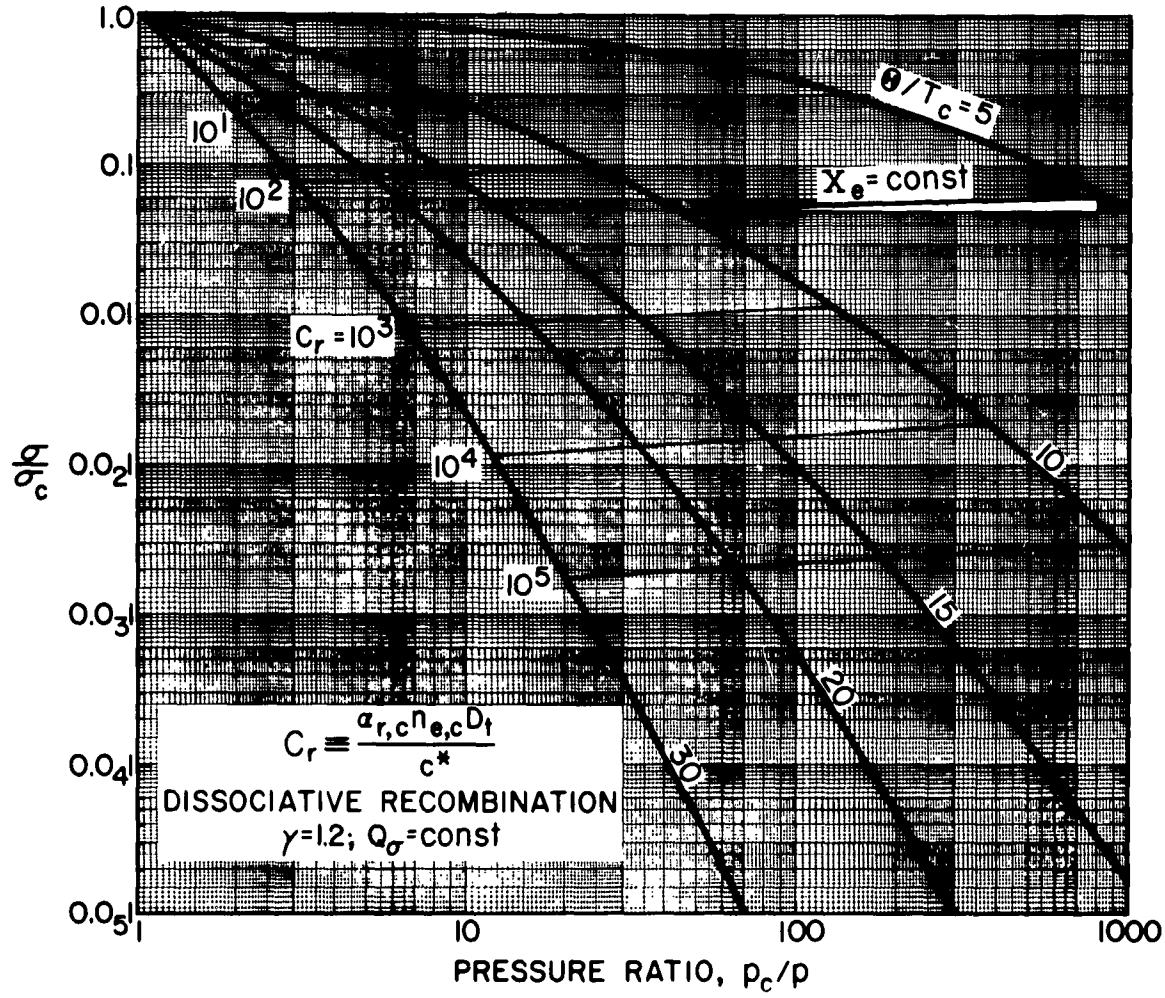

FIG. 5 THE EFFECT OF ELECTRON-ION RECOMBINATION LAG ON EXIT VALUES OF THE ELECTRICAL CONDUCTIVITY FOR ISENTROPIC NOZZLE EXPANSIONS

(γ = 1.2; Dissociative Recombination)

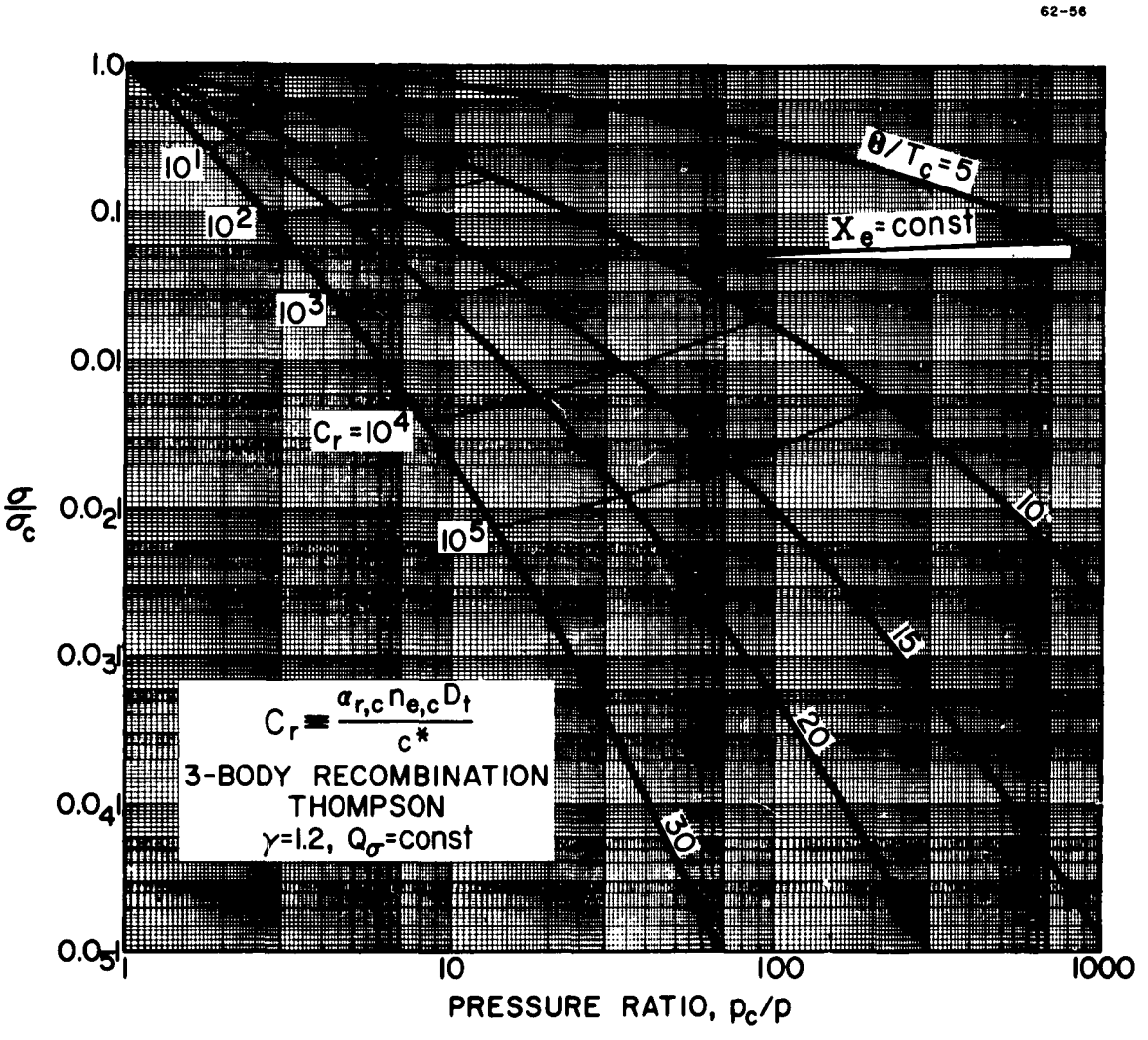

FIG. 6 THE EFFECT OF ELECTRON-ION RECOMBINATION LAG ON EXIT VALUES OF THE ELECTRICAL CONDUCTIVITY FOR ISENTROPIC NOZZLE EXPANSIONS

(γ = 1.2; Thompson Recombination)

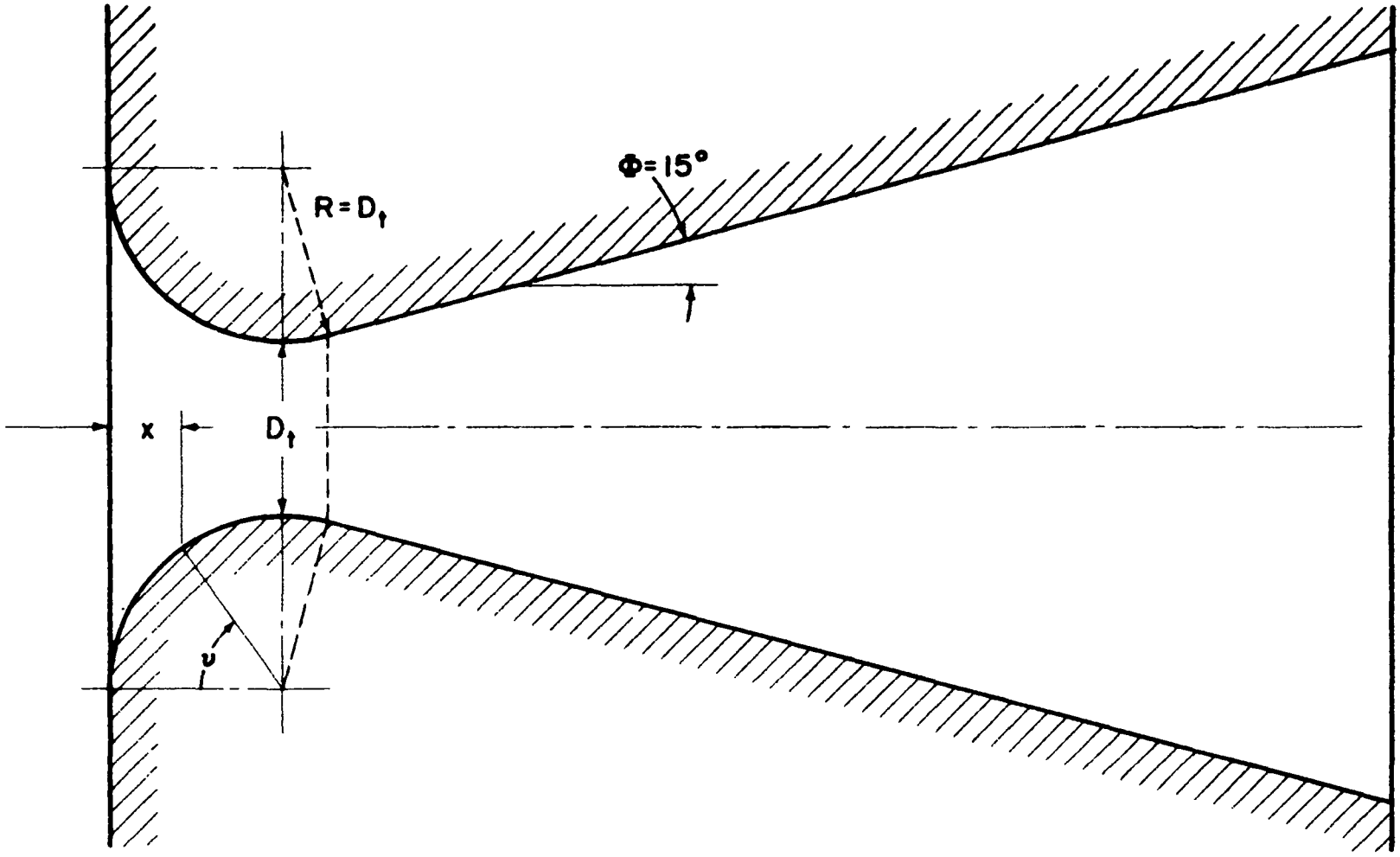

FIG. 7 NOZZLE SHAPE TREATED IN RECOMBINATION STUDY

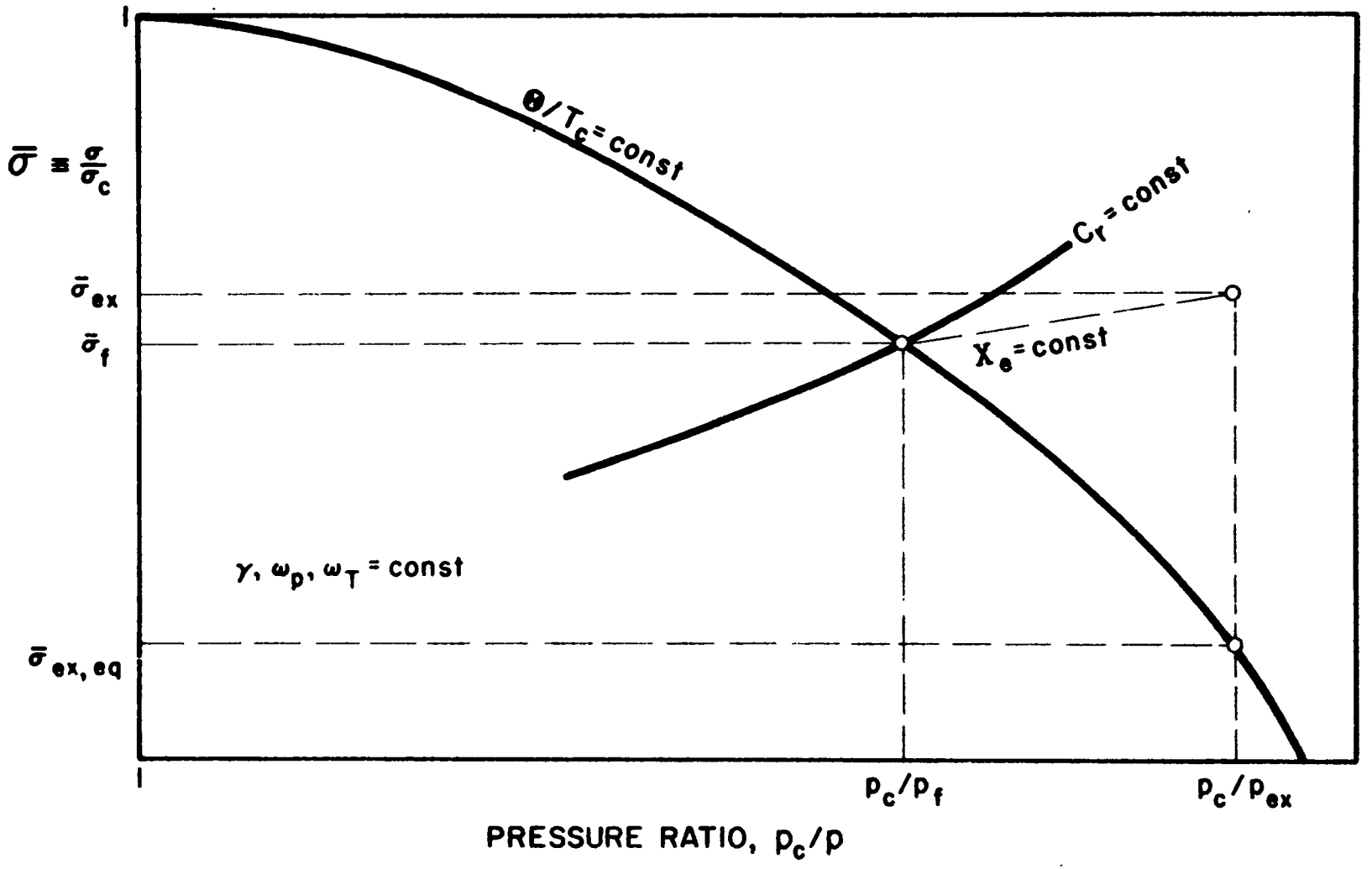

FIG. 8 GRAPHICAL DETERMINATION OF THE EFFECT OF IONIZATION NONEQUILIBRIUM ON EXIT VALUES OF THE ELECTRICAL CONDUCTIVITY FOR ISENTROPIC NOZZLE EXPANSIONS

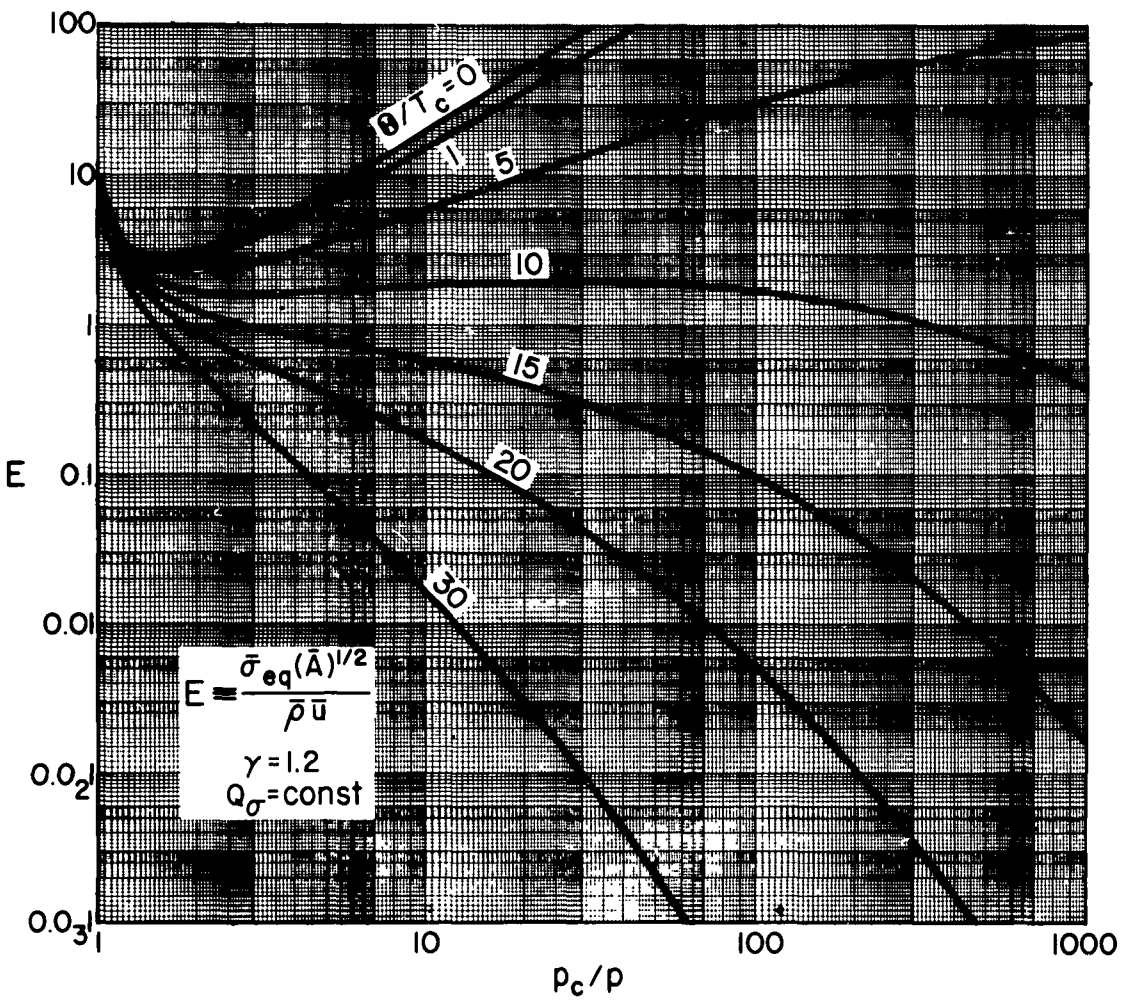

FIG. 9 PRESSURE DEPENDENCE OF EQUILIBRIUM EXPANSION FACTOR; (γ = 1.2)

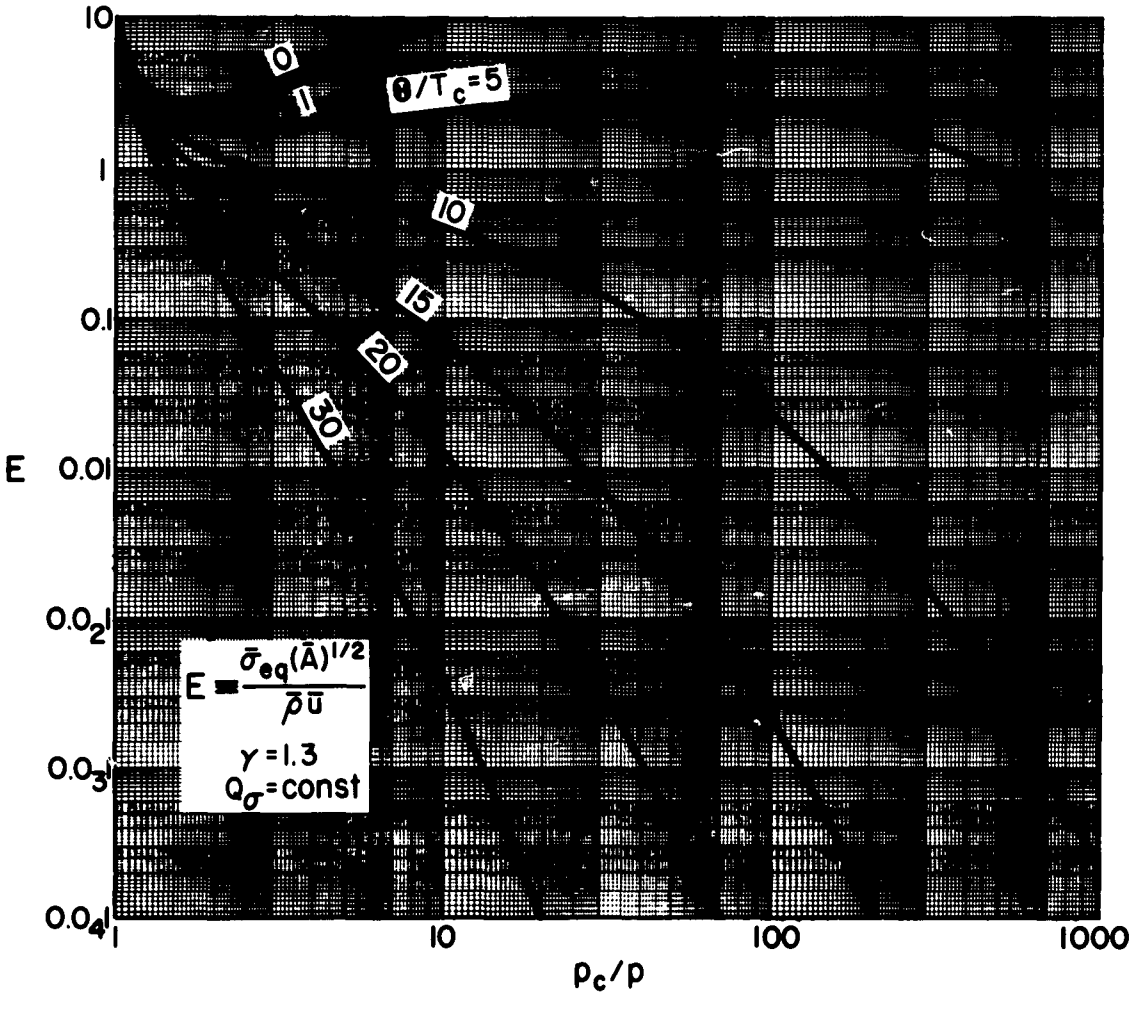

FIG. 10 PRESSURE DEPENDENCE OF EQUILIBRIUM EXPANSION FACTOR; (γ = 1.3)

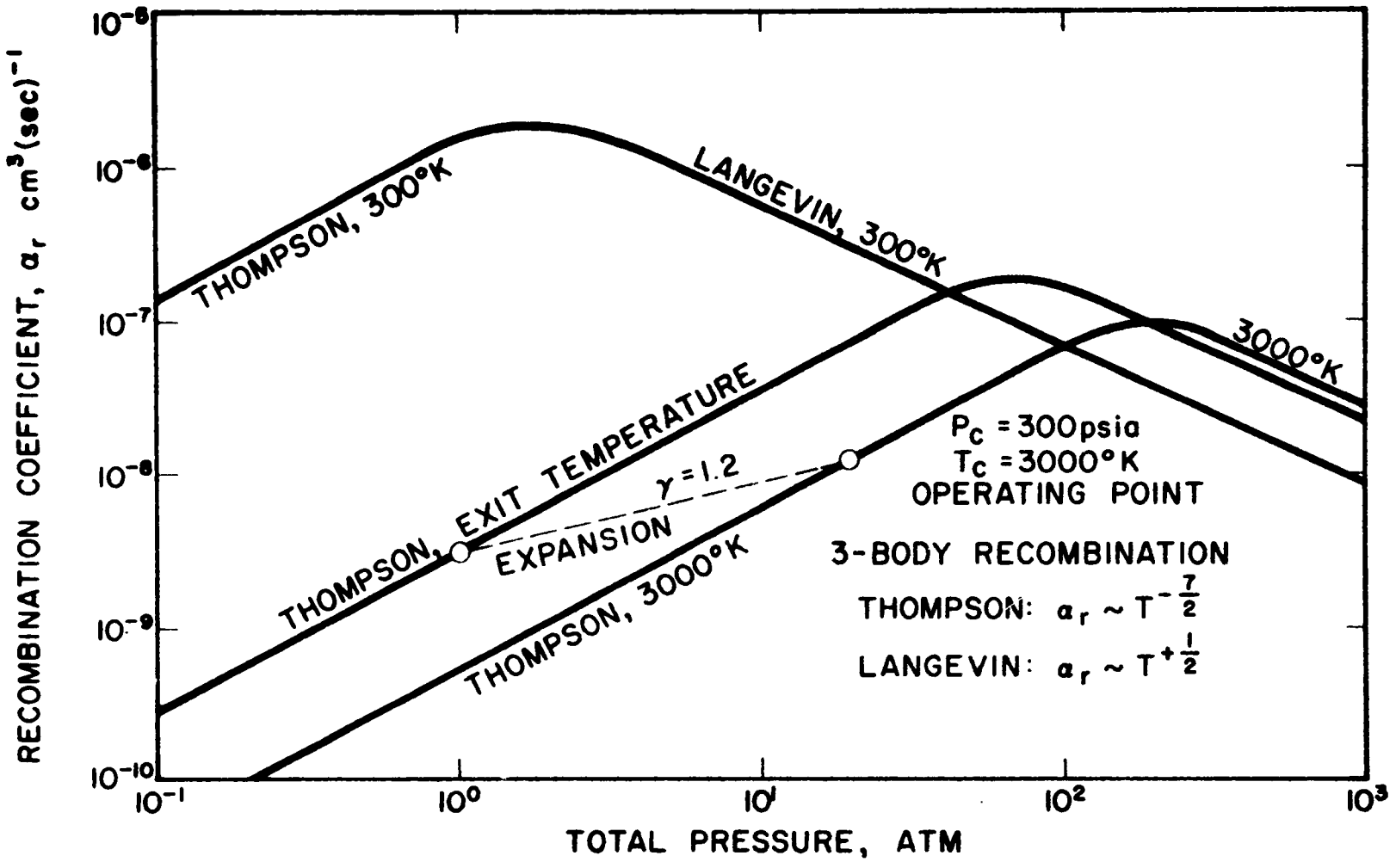

FIG. 11 PRESSURE DEPENDENCE OF THE ION RECOMBINATION COEFFICIENT FOR AIR

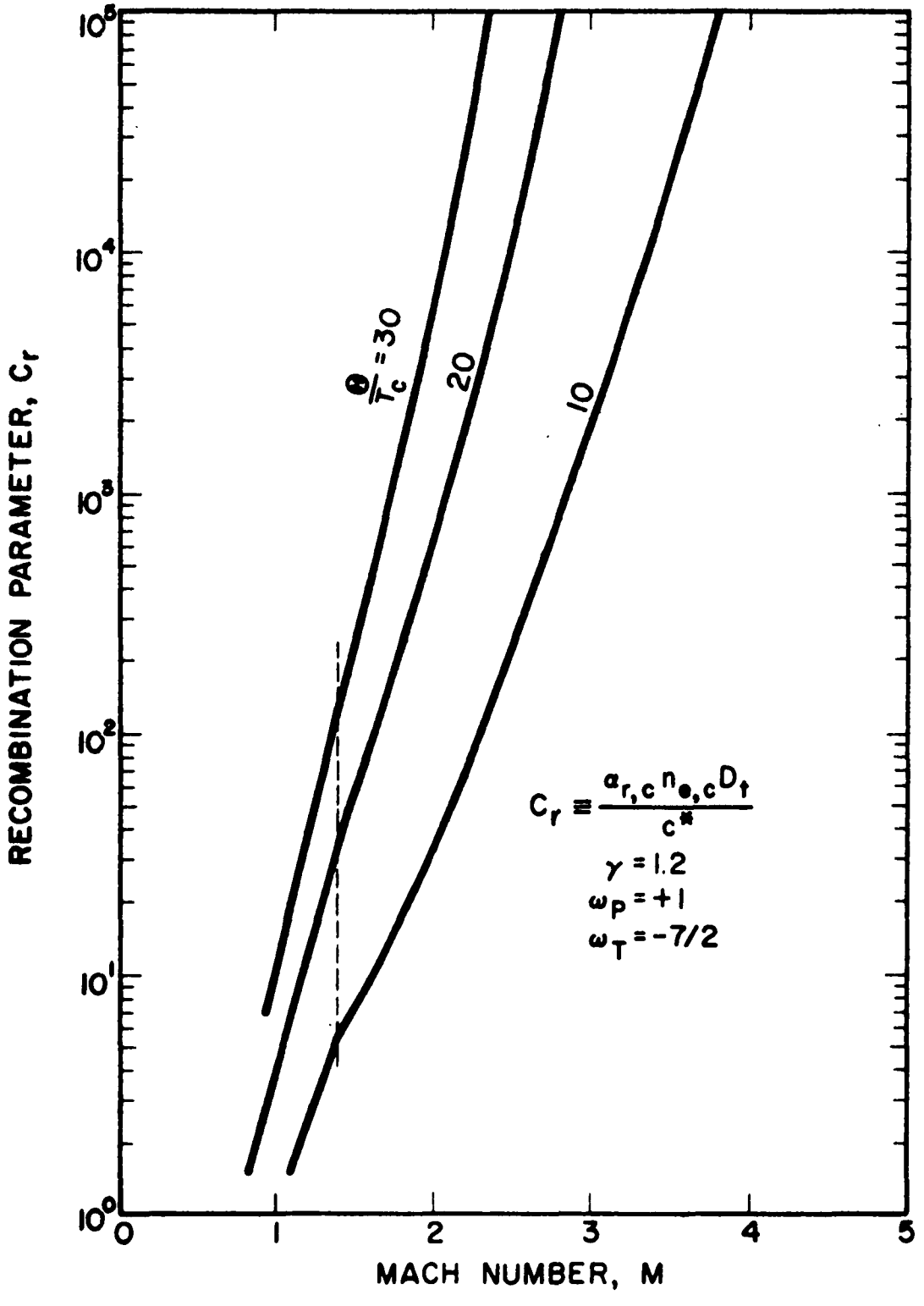

FIG. 12 LOCATION OF THE MACH NUMBER BEYOND WHICH THE ELECTRON MOLE FRACTION IS EXPECTED TO REMAIN UNCHANGED

(γ = 1.2; Thomoson Recombination)

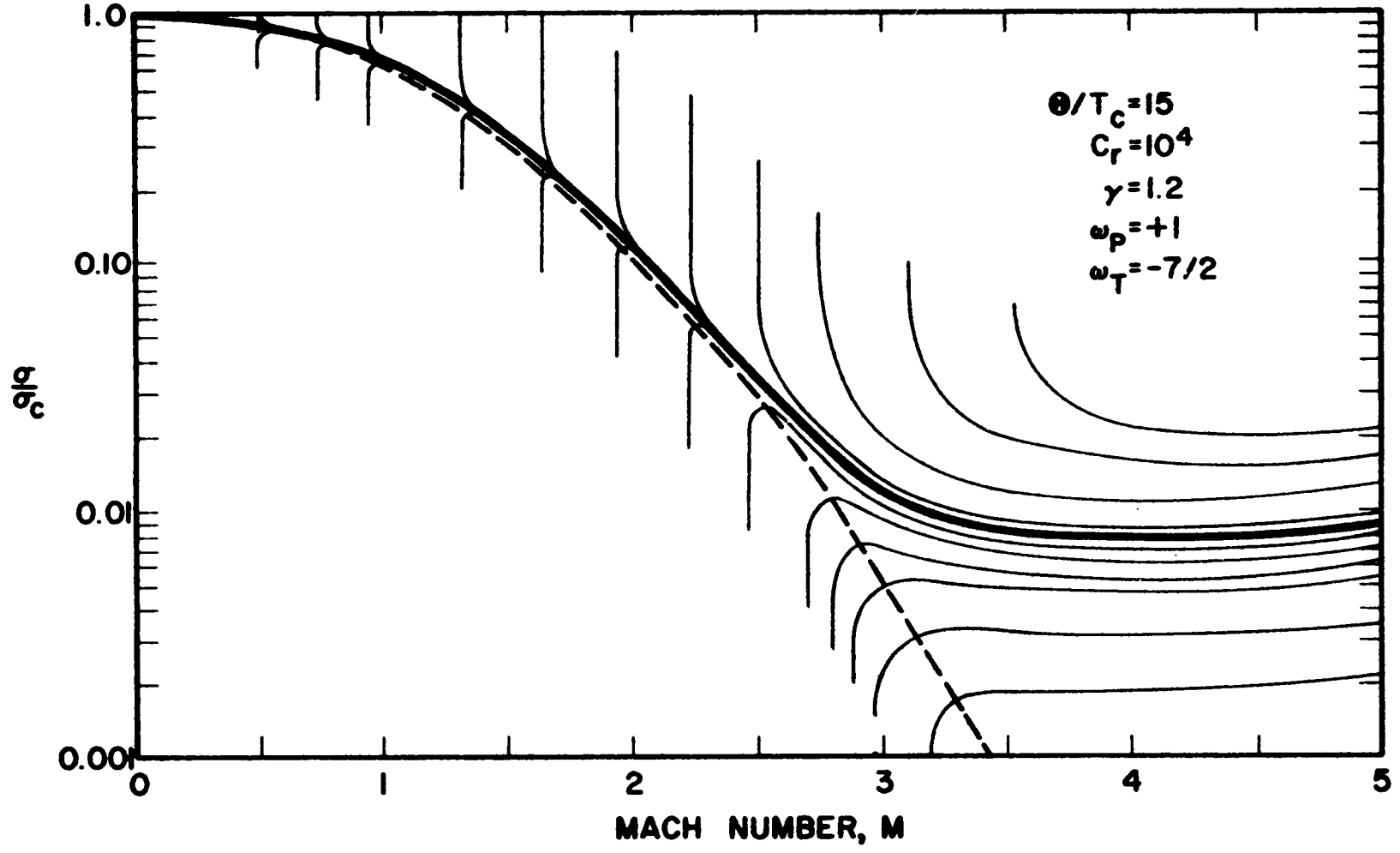

FIG. 13 EXACT INTEGRAL CURVES OF THE DIFFERENTIAL EQUATION GOVERNING CONDUCTIVITY CHANGES IN THE NOZZLE

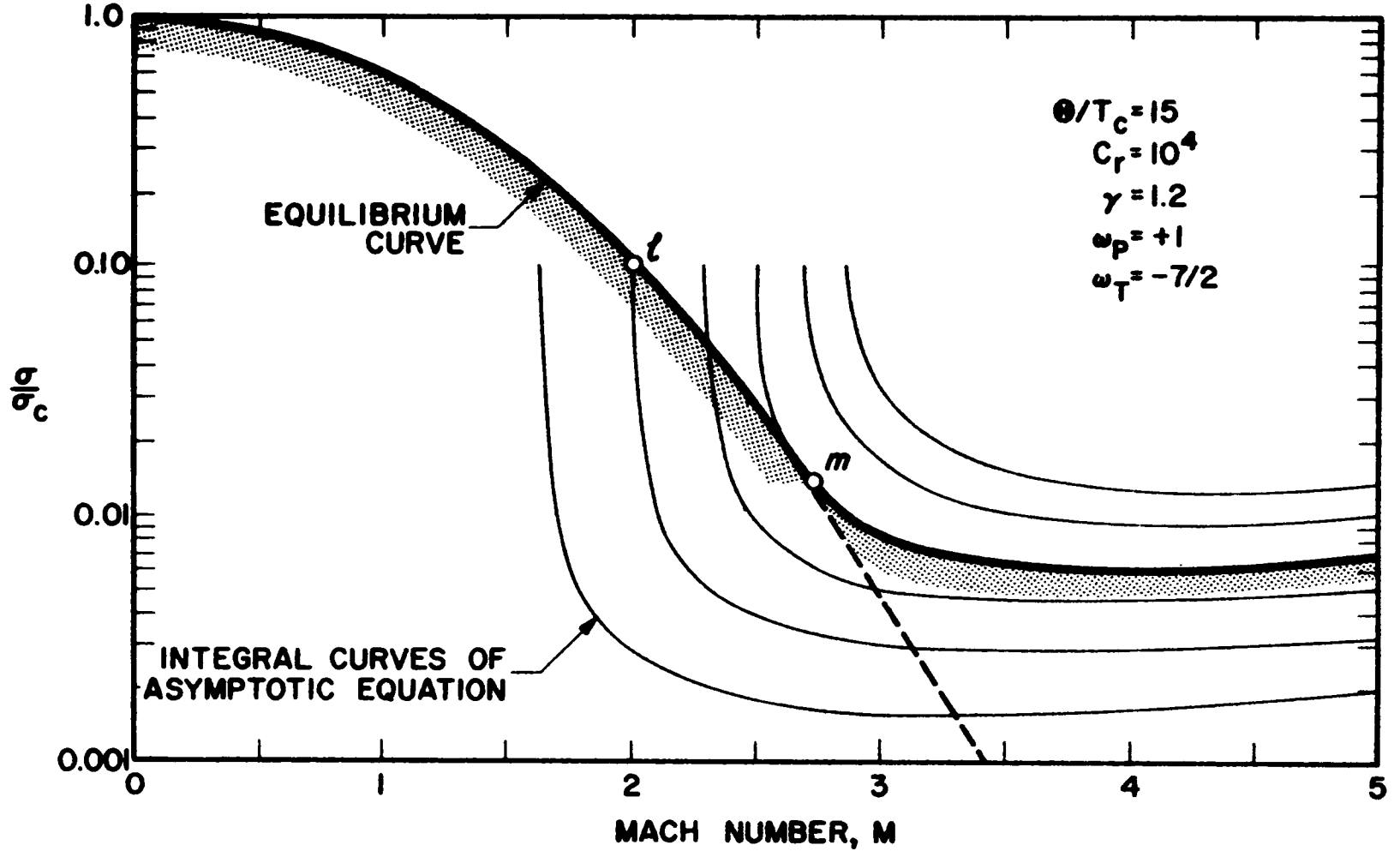

FIG. 14 IMPROVED APPROXIMATE SOLUTIONS; MAXIMUM LOWER BOUND TECHNIQUE

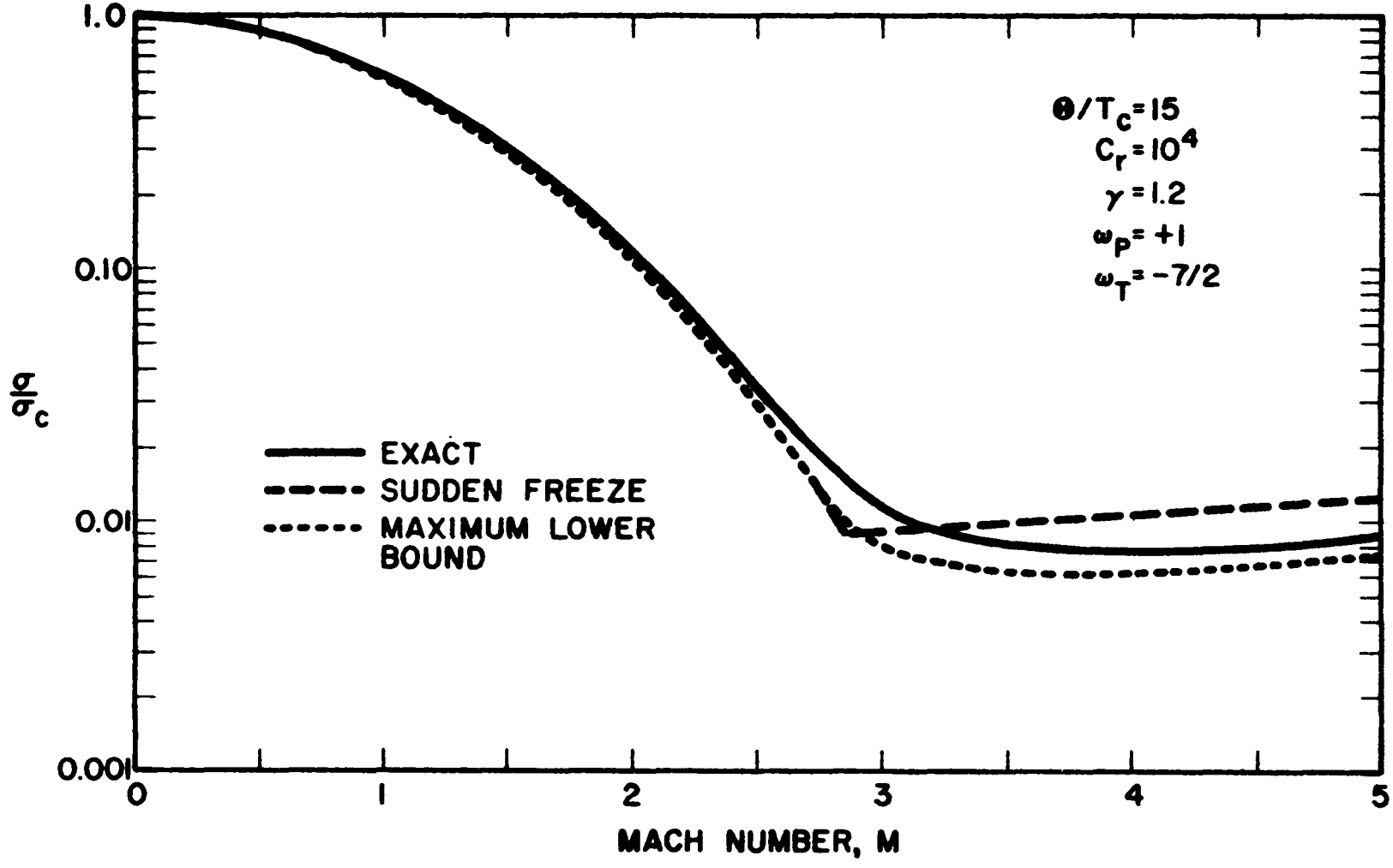

FIG. 15 COMPARISON OF EXACT AND APPROXIMATE SOLUTIONS FOR A PARTICULAR CASE
($\Theta/T_c = 15$, $C_r = 10^4$, $\gamma = 1.2$, $\omega_T = -7/2$, $\omega_p = +1$)

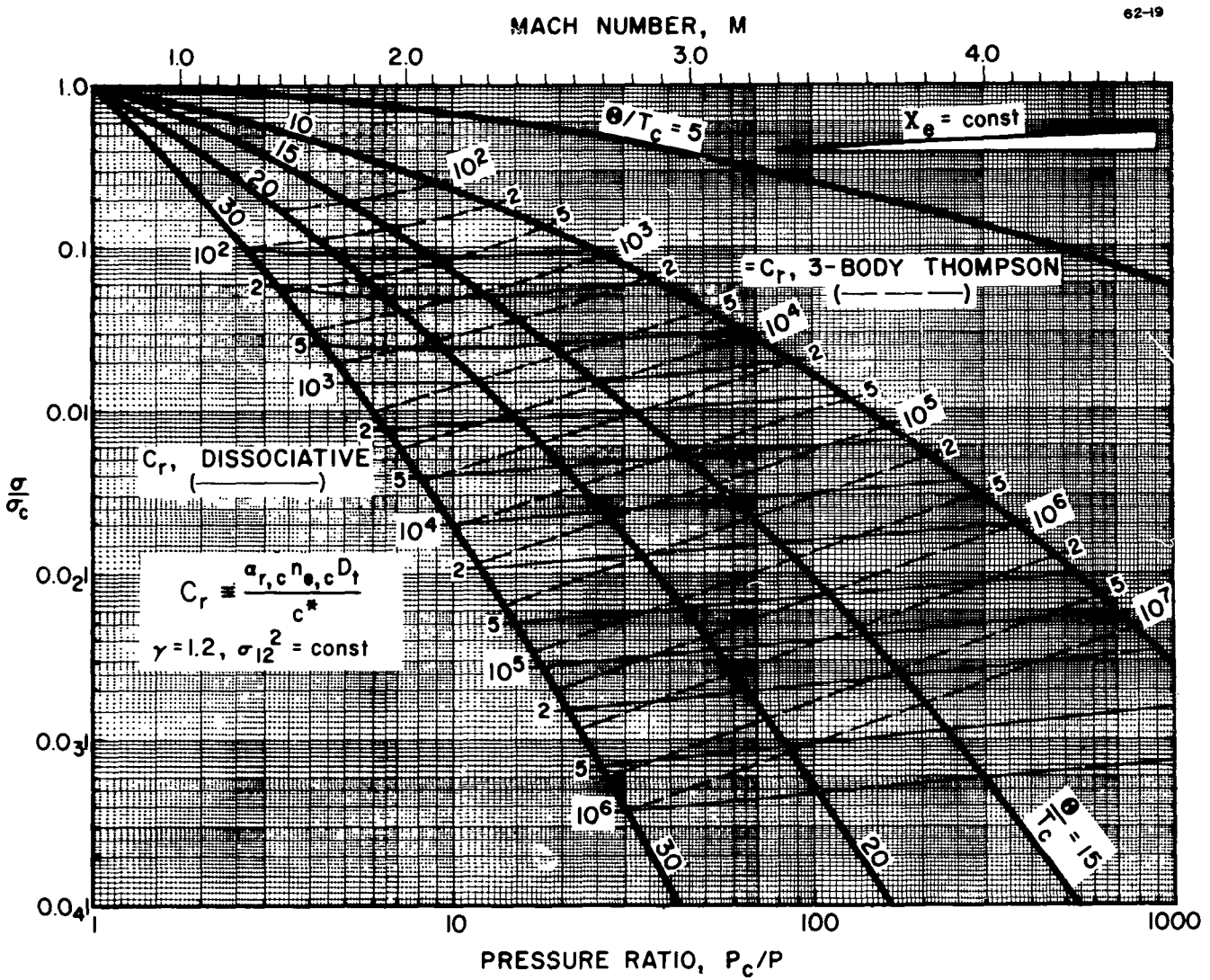

FIG. 16 MATCH POINTS ON THE LOG $\bar{\sigma}$ - LOG $\bar{p}^{-1}$ PLANE; MAXIMUM LOWER BOUND METHOD (γ = 1.2)

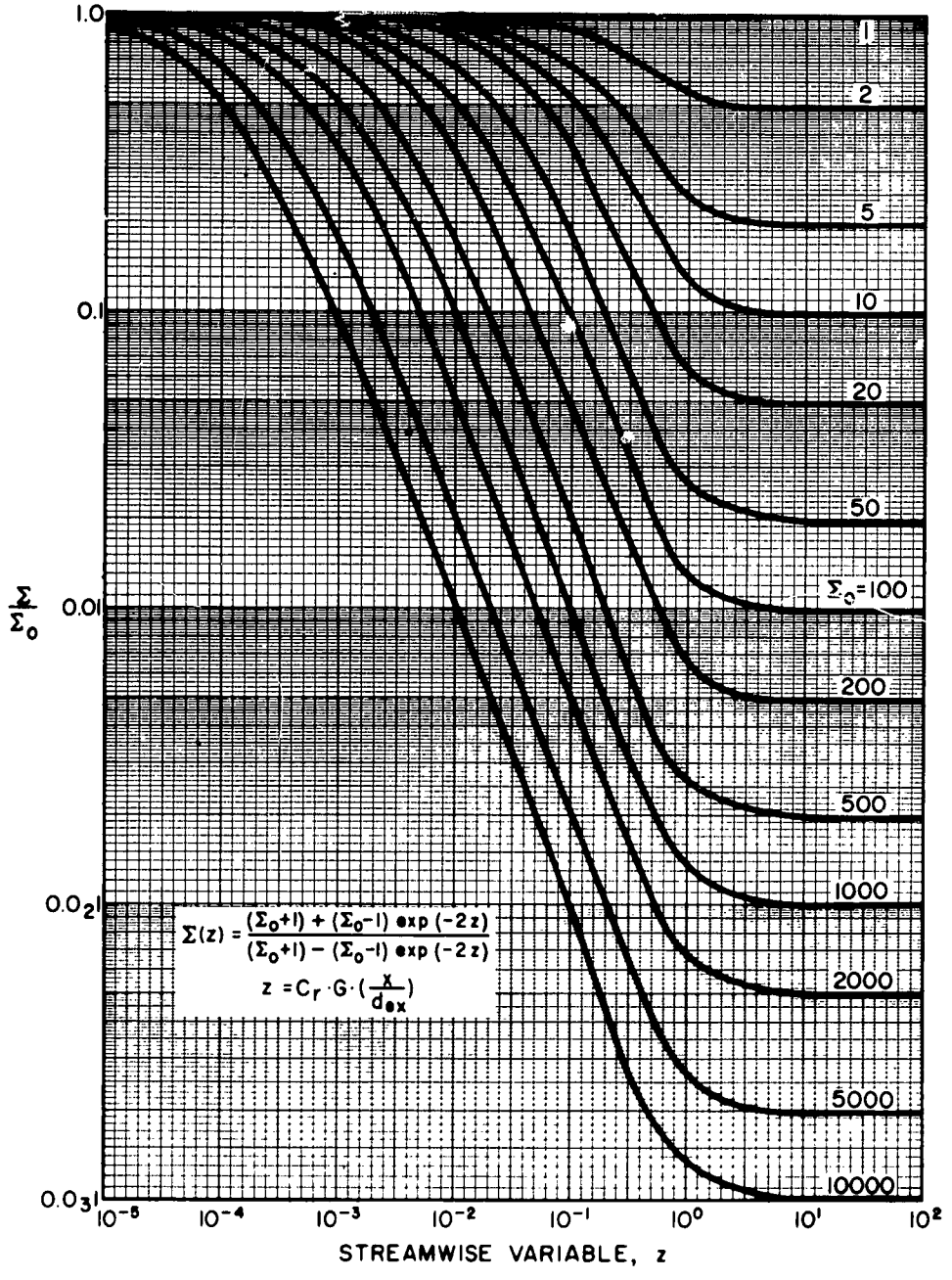

FIG. 17 DECAY OF ELECTRICAL CONDUCTIVITY DOWNSTREAM OF THE NOZZLE

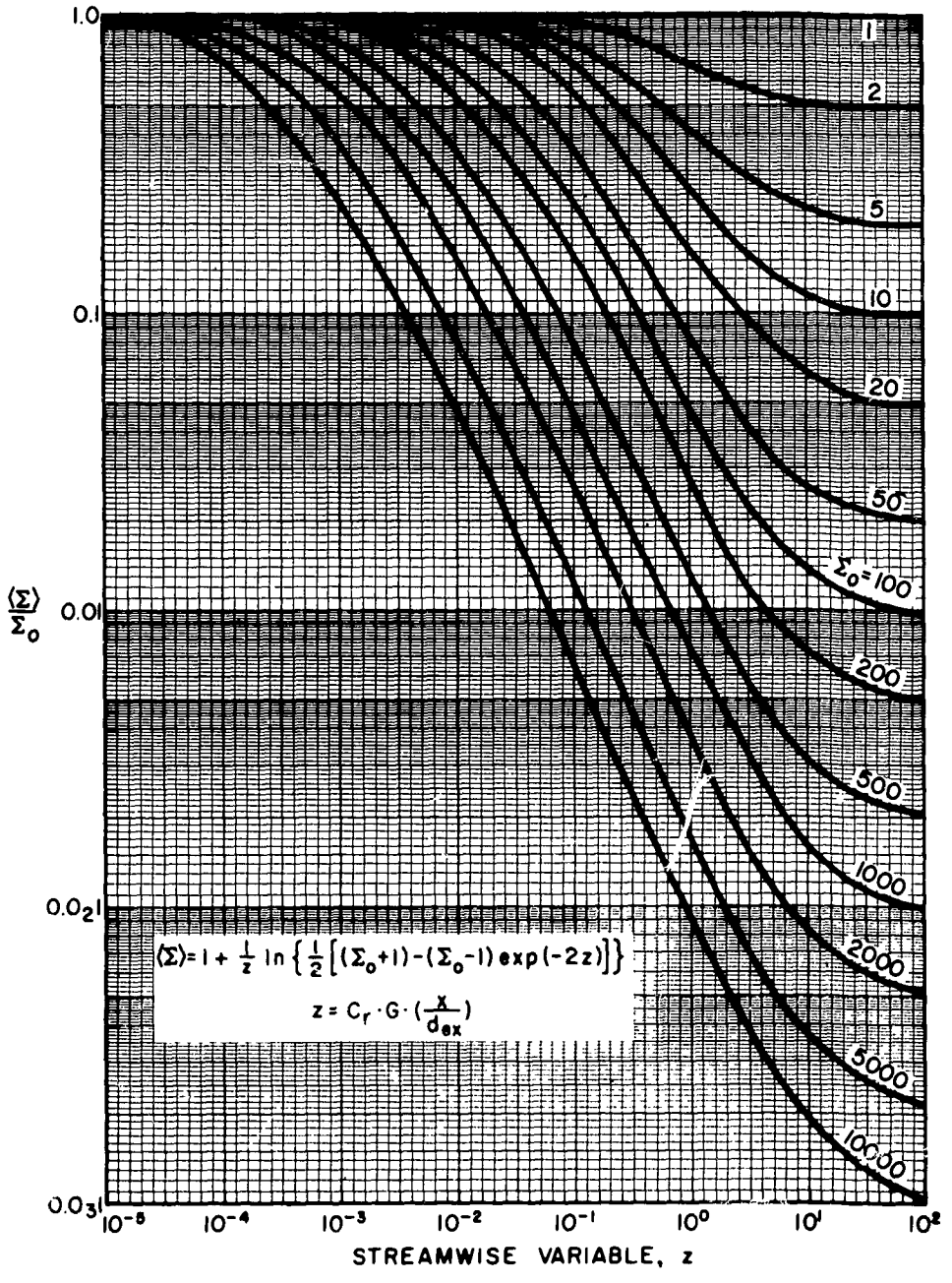

FIG. 18 DECAY OF SPATIALLY AVERAGED ELECTRICAL CONDUCTIVITY DOWNSTREAM OF THE NOZZLE

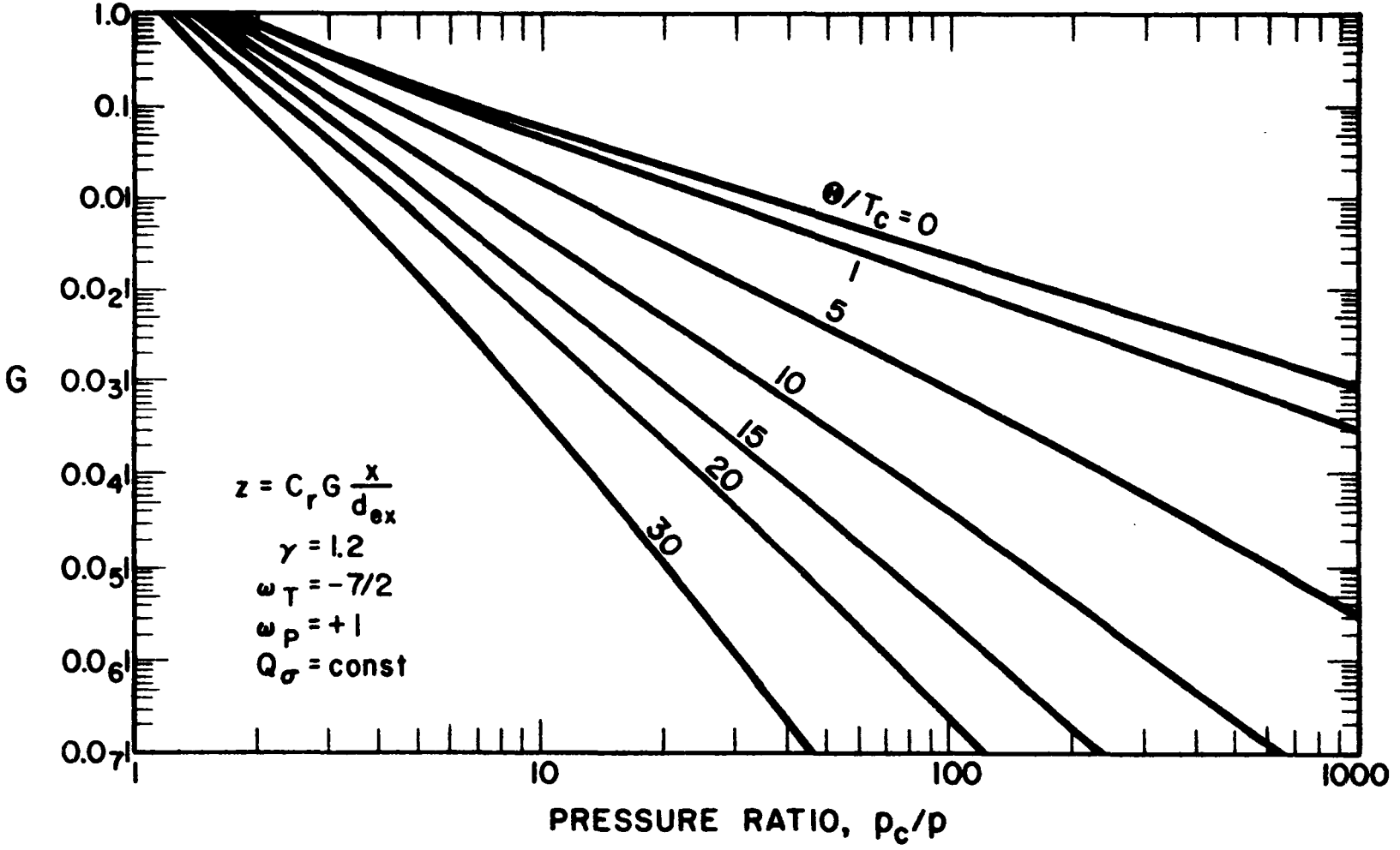

FIG. 19 UNIVERSAL FUNCTION REQUIRED TO CALCULATE THE STREAMWISE VARIABLE z FOR GIVEN VALUES OF C_r AND x/d_{ex}